11

Applications to Lattice Vibrations

Our first application of the space groups to excitations in periodic solids is in the area of lattice modes. Group theoretical techniques are important for lattice dynamics in formulating the normal mode secular determinant in block diagonal form, and symmetry is also important in determining the selection rules for optical processes involving lattice modes such as infrared and Raman activity. Transitions to lower symmetry through either phase transitions or *strain-induced* effects may lead to mode splittings. These mode splittings can be predicted using group theoretical techniques and the changes in the infrared and Raman spectra can be predicted. Another aim of this chapter is to consolidate some of the space group concepts of Chap. 9 on $\boldsymbol{r}$ space and Chap. 10 on $\boldsymbol{k}$ space with additional developments on both the fundamentals and applications of space groups.

11.1 Introduction

The atoms in a solid are in constant motion and give rise to lattice vibrations which are very similar to the molecular vibrations which we have discussed in Chap. 8. We discuss in this section and in Sect. 11.2 the similarities and differences between lattice modes and molecular vibrations.

Suppose that we have a solid with N atoms which crystallize into a simple Bravais lattice with 1 atom/unit cell. For this system there are $3N$ degrees of freedom corresponding to three degrees of freedom/atom for the molecular system or three degrees of freedom/primitive unit cell for simple crystalline solids. There are N allowed wave vector states in the Brillouin zone which implies that there are three branches for the phonon dispersion curves of a simple monatomic solid, each branch containing solutions for N $\boldsymbol{k}$-vectors. For the case of molecules, we subtract three degrees of freedom corresponding to the uniform translation of the molecule. In the crystalline solid, these uniform translational modes correspond to the acoustic modes at $\boldsymbol{k} = 0$, which are subject to the constraint that

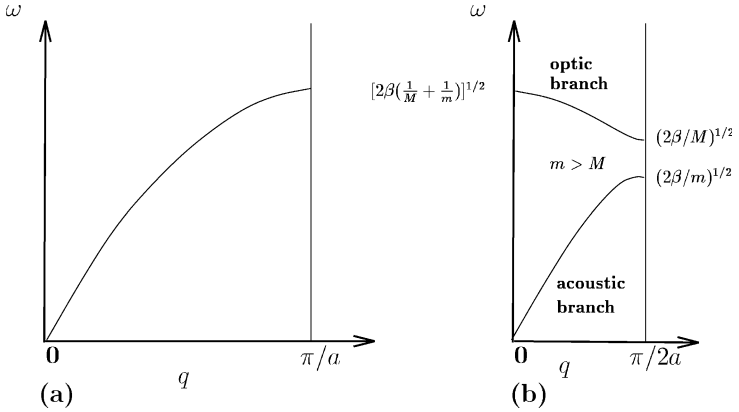

Fig. 11.1. Phonon dispersion curves for a one-dimensional line of atoms with (**a**) a single mass and (**b**) two different masses m and M

$\omega^2_{\text{acoustic}} \equiv 0$ as $k \to 0$. The three modes corresponding to the rotations of the solid about the *center* of mass are not specifically considered here.

We have found in Chap. 10 that the translational symmetry of a crystal is conveniently handled by *labeling* the N irreducible representations of the translation group by the N $\boldsymbol{k}$ vectors which are accommodated in the 1st Brillouin zone. So if we have a primitive unit cell with 1 atom/unit cell, there are three vibrational modes for each $\boldsymbol{k}$ value and together these three modes constitute the acoustic branches. In particular, there are three acoustic vibrational modes for the $\boldsymbol{k} = 0$ wave vector, which exhibits the full point group symmetry of the crystal; these three acoustic modes correspond to the pure *translational modes* which have zero frequency and zero restoring force.

We review here the phonon dispersion relations in a one-dimensional crystal with 1 atom/unit cell (see Fig. 11.1(a)) and with 2 atoms/unit cell (see Fig. 11.1(b)) having masses m and M where $m < M$, and a is the distance between adjacent atoms. For the acoustic branch at $\boldsymbol{k} = 0$, all atoms vibrate in phase with identical displacements u along the direction of the atomic chain, thus corresponding to a pure translation of the chain. The wave vector $\boldsymbol{k}$ distinguishes each normal mode of the system by introducing a phase factor e^{ika} between the displacements on adjacent sites. For the case of one atom/unit cell, the lattice mode at the zone boundary corresponds to atoms moving 90° out of phase with respect to their neighbors. For the case of 2 atoms/unit cell, the size of the unit cell is twice as large, so that the size of the corresponding Brillouin zone (B.Z.) is reduced by a factor of 2. The dispersion relations and lattice modes in this case relate to those for one atom/unit cell by a zone folding of the dispersion relation shown in Fig. 11.1(a), thus leading to Fig. 11.1(b). Thus the optical mode at $\boldsymbol{k} = 0$ has *neighboring* atoms moving out of phase with respect to each other. The normal mode at the new B.Z.

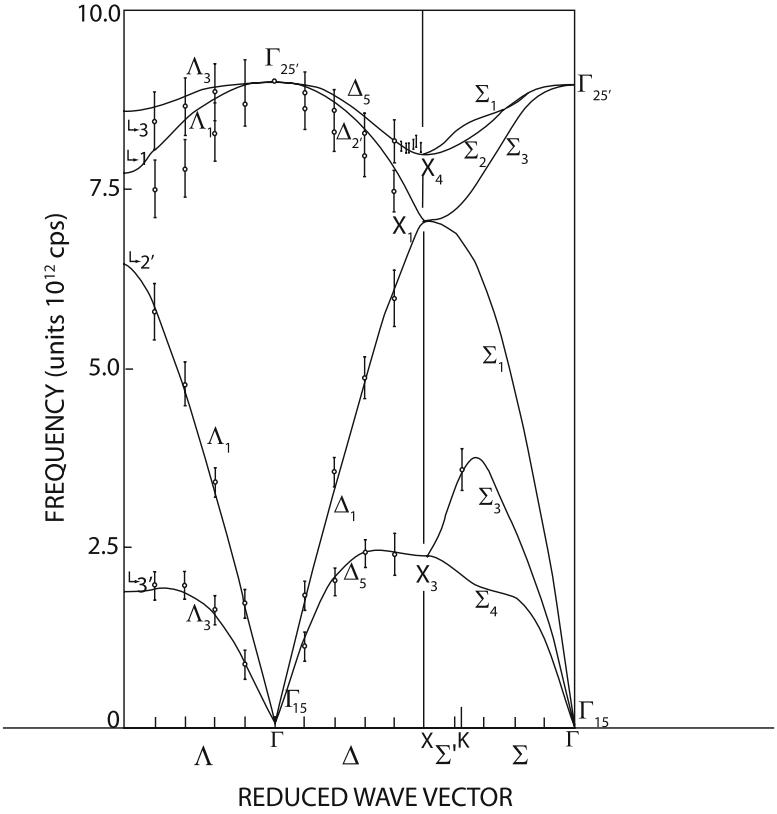

Fig. 11.2. Phonon dispersion curves for Ge along certain high symmetry axes in the Brillouin zone. The data at the Γ point are from Raman scattering measurements and the data elsewhere in the zone are from neutron scattering experiments [28]

boundary $k = \pi/2a$ thus corresponds to a mode where one atom is at rest, while its neighbor is in motion.

In three-dimensions, the phonon dispersion relations for Ge with the diamond structure (with 2 atoms/unit cell) are plotted along high symmetry directions in Fig. 11.2 and the dispersion relations are *labeled* by the appropriate irreducible representations by giving the symmetry of the corresponding normal mode (see Chap. 10 for the notation used in Fig. 11.2). The phonon dispersion relations for *germanium* are determined from inelastic neutron scattering measurements and are plotted as points in Fig. 11.2. At a general point k in the B.Z. for the diamond structure, there are three acoustic branches and three optical branches. However, at certain high symmetry points and along certain high symmetry directions, mode degeneracies occur as, for example, along ΓL and ΓX. Group theory allows us to identify the high symmetry points in the B.Z. where degeneracies occur, which branches stick together,

which branches show simple mode crossings, and which modes show anticrossings, [12–14, 28, 30] (see Fig. 10.5), to be discussed further in this chapter.

The symmetry aspects of the lattice mode problem at $\boldsymbol{k} = 0$ for simple structures with 1 atom/unit cell are simply the uniform translation of the solid. However, group theory is needed to deal with lattice modes away from $\boldsymbol{k} = 0$. Furthermore, the lattice modes that are of interest in the current literature often involve complicated crystal structures with many atoms/unit cell or systems with reduced dimensionality; for such problems, group theory is a powerful tool for lattice mode classification and for the determination of selection rules for infrared and Raman spectroscopy and for phonon-assisted optical transitions more generally.

The *general outline* for procedures that utilize group theory to solve for the lattice modes in solids is as follows:

1. Find the symmetry operations for the group of the wave vector $\boldsymbol{k} = 0$, the appropriate character table and irreducible representations.
2. Find the irreducible representations using $\Gamma_{\text{lat. mod.}} = \Gamma^{\text{equiv.}} \otimes \Gamma_{\text{vector}}$. The meaning of this relation is discussed below (item (c) in Sect. 11.2). We will use $\Gamma_{\text{lat.mod.}}$ to denote $\Gamma_{\text{lattice modes}}$.
3. Find the irreducible representations of $\Gamma_{\text{lat.mod.}}$. The characters for the lattice mode representation express the symmetry types and degeneracies of the lattice modes.
4. Find the normal mode patterns.
5. Which modes are IR-active? Which modes are Raman-active? Are there any polarization effects?
6. Repeat items 1–4 for other points in the Brillouin zone and find the lattice for $k \neq 0$.
7. Using the compatibility relations, connect up the lattice modes at neighboring $\boldsymbol{k}$ points to form a phonon branch.

11.2 Lattice Modes and Molecular Vibrations

There are several aspects of the lattice mode problem in the crystalline phase that differ from simple molecular vibrations (see Sect. 8.2):

(a) *The eigenvectors and normal modes.* In the lattice mode problem, we consider normal modes for the atoms in a unit cell rather than for a molecule, and in either case the lattice mode is one form of a basis vector or eigenvector (see Chap. 4). Since the symmetry is different for the various types of $\boldsymbol{k}$-vectors in the Brillouin zone, we must solve the lattice mode problem for each distinct type of $\boldsymbol{k}$-vector. On the other hand, for many experimental studies of the lattice modes, we use light as our probe. Usually the main interest is in lattice modes at or near $\boldsymbol{k} = 0$ (the Γ point) because the wavelength of light is long ($\lambda \approx 500\,\text{nm}$) compared to lattice constants a, and the magnitude of the corresponding $\boldsymbol{k}$ wavevector ($k = 2\pi/\lambda$) is very

small compared with Brillouin zone dimensions ($2\pi/a$, $a \sim 0.1$–$1.0\,\mathrm{nm}$). Most of our simple examples, therefore emphasize the lattice modes for $\boldsymbol{k} = 0$.

(b) *Equivalence.* To find the equivalence transformation $\Gamma^{\text{equiv.}}$ for molecules, we consider the action of a symmetry operator $\hat{P}_R$ on an atomic site and examine the transformation matrix to see whether or not the site is transformed into itself under the point symmetry operation $\hat{P}_{R_\alpha}$. In the case of a crystal, however, we consider all points separated by a lattice vector $\boldsymbol{R}_n$ as identical when considering Γ point ($k = 0$) phonons. Thus $\boldsymbol{r} \rightarrow \boldsymbol{r} + \boldsymbol{R}_n$ is an *identity transformation* for all $\boldsymbol{R}_n$. and therefore we denote the equivalence transformation in crystalline solids by $\Gamma^{\text{equiv.}}$ and the corresponding characters of this representation by $\chi^{\text{equiv.}}$. Compound operations in nonsymmorphic groups always give $\chi^{\text{equiv.}} = 0$ since the translation $\boldsymbol{\tau}_\alpha$ is not a lattice vector. When considering lattice modes away from the Γ point, we must consider the group of the wavevector G_k and phase factors related to translations. Modes away from $k = 0$ are discussed in Sect. 11.4.

(c) *Degrees of freedom and phonon branches.* For the case of molecular vibrations, we have

$$\Gamma_{\text{mol. vib.}} = \Gamma^{\text{equiv.}} \otimes \Gamma_{\text{vec}} - \Gamma_{\text{trans}} - \Gamma_{\text{rot}}\,, \tag{11.1}$$

whereas for lattice modes (lat. mod.), we simply write

$$\Gamma_{\text{lat. mod.}} = \Gamma^{\text{equiv.}} \otimes \Gamma_{\text{vec}}\,. \tag{11.2}$$

That is, we do not subtract $\Gamma_{\text{trans.}}$ and $\Gamma_{\text{rot.}}$ in (11.2) for the lattice modes for the following reasons. Each atom/unit cell has three degrees of freedom, yielding a normal mode for each wave vector $\boldsymbol{k}$ in the Brillouin zone. The collection of normal modes for a given degree of freedom for all $\boldsymbol{k}$ vectors forms a *phonon branch.* Thus for a structure with one atom/unit cell there are three phonon branches, the acoustic branches. If there is more than 1 atom/unit cell, then

$$\text{no. of branches} = (\text{no. of atoms/unit cell}) \times 3 \tag{11.3}$$

of which three are acoustic branches and the remainder are optical branches. The translational degrees of freedom correspond to the trivial $\boldsymbol{k} = 0$ solution for the three acoustic branches which occur at $\omega = 0$ and are smoothly connected with nontrivial solutions as we move away from the Γ point. Since the atoms in the solid are fixed in space, there are no rotational degrees of freedom to be subtracted.

We will now illustrate the application of group theory to the solution of the lattice mode problem for several illustrative structures. First we consider simple symmorphic structures in Sect. 11.3. Then we consider some simple nonsymmorphic structures (see Sect. 11.3.3). Our initial examples will be for the $\boldsymbol{k} = 0$ modes. This will be followed by a discussion of modes elsewhere in the Brillouin zone.

11.3 Zone Center Phonon Modes

In this section we consider the symmetries of zone center phonon modes for some illustrative cases. The examples selected in this section are chosen to demonstrate some important aspect of the lattice mode problem and to gain some experience in using simple space groups.

11.3.1 The NaCl Structure

The NaCl structure is shown in Fig. 9.6(b). This very simple example is selected to illustrate how the symmetries of the lattice modes are found. We take our "basic unit cell" to be the primitive rhombohedral unit cell of either one of the inter-penetrating FCC structures (space group #225 ($Fm3m$) O_h^5), so that each primitive unit cell will contain an Na atom and a Cl atom. The larger cubic unit cell (Fig. 9.6(b)) contains four primitive unit cells with four Na and four Cl atoms (ions). The space group O_h^5 for the NaCl structure is a symmorphic structure, and the group of the wave vector at $\boldsymbol{k} = 0$ for the NaCl structure is O_h. Since the details of the translations do not enter into the considerations of phonons at $\boldsymbol{k} = 0$ for symmorphic space groups, we need to consider only point group operations for O_h as given in Table 10.2. Under all symmetry operations of O_h each Na and Cl atom site is transformed either into itself or into an equivalent atom site separated by a lattice vector $\boldsymbol{R}_m$. Thus,

$$\Gamma^{\text{equiv.}} = 2\Gamma_1\,. \tag{11.4}$$

For O_h symmetry, $\Gamma_{\text{vec.}} = \Gamma_{15}$, so that at $\boldsymbol{k} = 0$

$$\Gamma_{\text{lat. mod.}} = 2\Gamma_1 \otimes \Gamma_{15} = 2\Gamma_{15}\,, \tag{11.5}$$

where the basis functions for Γ_{15} are (x, y, z). Thus both the acoustic branch and the optic branch at $\boldsymbol{k} = 0$ have Γ_{15} (or Γ_{15}^-) symmetry. The normal modes for the acoustic branches of the NaCl structure have both the Na and Cl atoms moving in phase in the x, y, and z directions, while for normal

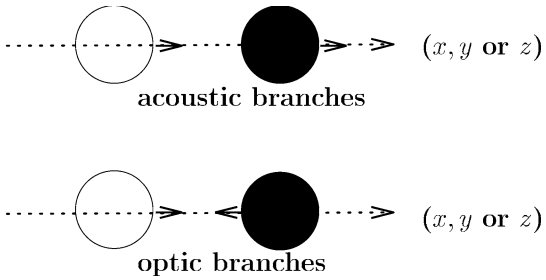

Fig. 11.3. In-phase (acoustic) and out-of-phase (optic) normal modes at $\boldsymbol{k} = 0$ for NaCl

modes in the optic branches, the two atoms move out of phase in the x, y, and z directions (see Fig. 11.3). Since the electromagnetic interaction transforms as the vector (Γ_{15}), the optic branch is infrared-active. The acoustic branch is not optically excited because $\omega = 0$ at $\boldsymbol{k} = 0$. Since the optic branch for the NaCl structure has odd parity, it is not Raman-active. As we move away from the Γ point ($\boldsymbol{k} = 0$), the appropriate symmetries can be found by compatibility relations. For example along the (100) directions $\Gamma_{15} \rightarrow \Delta_1 + \Delta_5$ in which Δ_1 is the symmetry of the longitudinal mode and Δ_5 is that for the doubly degenerate transverse modes. We will now give several other examples of zone center modes in other structures and then return in Sect. 11.4 to the discussion of nonzone-center modes for simple structures.

11.3.2 The Perovskite Structure

Let us now consider lattice modes in $BaTiO_3$ (see Fig. 9.7(c)), an example of a cubic crystal structure with slightly more complexity, but still corresponding to a symmorphic space group. The focus of this section is to illustrate the identification of the normal modes. For the perovskite structure shown in Fig. 9.7(c), there are 5 atoms/unit cell and therefore there are 15 degrees of freedom, giving rise to three acoustic branches and twelve optical branches. The point group of symmetry at $\boldsymbol{k} = 0$ is O_h. Consider the unit cell shown in Fig. 11.4. The Ba^{2+} ions at the cube corners are shared by eight neighboring unit cells, so that one Ba^{2+} ion is considered to be associated with the unit cell shown. Likewise the O^{2-} ions in the face centers are shared by two unit cells, so that $3O^{2-}$ ions are treated in the unit cell shown. The Ti^{4+} ion at the cube center is of course fully contained in the unit cell shown in Fig. 11.4.

Using the diagram in Fig. 11.4, we thus obtain Character Table 11.1 for $\Gamma^{\text{equiv.}}$. From the character table for O_h (see Table A.31) we see that

$$\Gamma^{\text{equiv.}} = 3\Gamma_1^+ + \Gamma_{12}^+ \,. \tag{11.6}$$

We note that the Ba^{2+} and Ti^{4+} ions each transform as Γ_1^+ with the three oxygens transforming as $\Gamma_1 + \Gamma_{12}$. In O_h symmetry

$$\Gamma_{\text{vec.}} = \Gamma_{15}^- \,, \tag{11.7}$$

so that

$$\Gamma_{\text{lat.mod.}} = (3\Gamma_1^+ + \Gamma_{12}^+) \otimes \Gamma_{15}^- = 3\Gamma_{15}^- + (\Gamma_{12}^+ \otimes \Gamma_{15}^-) \tag{11.8}$$

$$= 4\Gamma_{15}^- + \Gamma_{25}^- = 4\Gamma_{15}^- + \Gamma_{25}^- \,. \tag{11.9}$$

Table 11.1. Characters for Γ_{equiv} for perovskite. The atoms that remain unchanged under each symmetry operation are indicated

	E	$8C_3$	$3C_4^2$	$6C_2'$	$6C_4$	i	$8iC_3$	$3iC_4^2$	$6iC_2'$	$6iC_4$
$\Gamma^{\text{equiv.}}$	5	2	5	3	3	5	2	5	3	3
	all	Ba,Ti	all	Ba,Ti one O	Ba,Ti one O	all	Ba,Ti	all	Ba,Ti one O	Ba,Ti one O

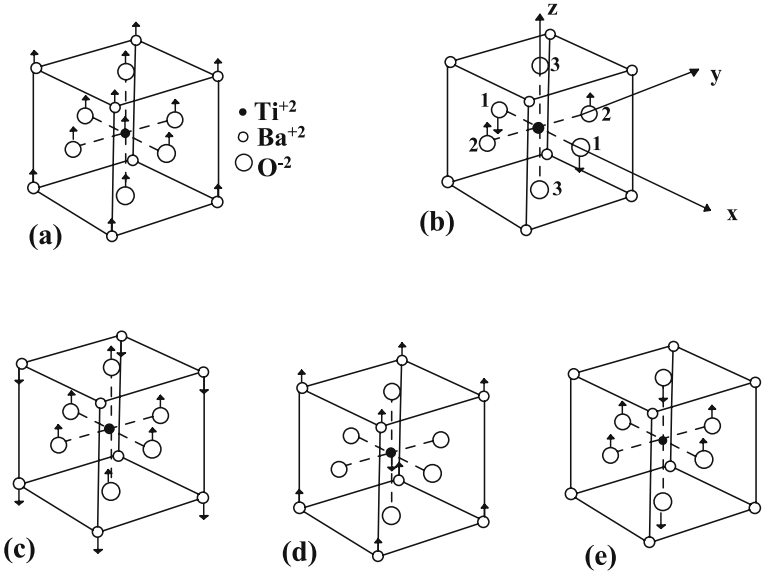

Fig. 11.4. Schematic diagram of the z-component lattice modes at $\boldsymbol{k} = 0$ for the $BaTiO_3$ perovskite structure. (**a**) Γ_{15} acoustic mode; (**b**) Γ_{25} mode where only two of the three distinct oxygens move; (**c**) Γ_{15} mode with the Ti^{4+} and Ba^{2+} vibrating against the oxygens. (**d**) Γ_{15} mode with the Ti^{4+} vibrating against the Ba^{2+} and (**e**) Γ_{15} breathing mode of the transverse oxygens vibrating against the longitudinal oxygens, while the Ti^{4+} and Ba^{2+} are at rest

where we note that both Γ_{15}^- and Γ_{25}^- have odd parity. Thus at $\boldsymbol{k} = 0$ there are five distinct normal mode frequencies, including the acoustic branch with Γ_{15}^- symmetry and $\omega = 0$. Since the atom sites for the Ba^{2+} and Ti^{4+} ions transform as Γ_1^+, we know that the Γ_{25} mode requires motion of the oxygens. In the following we illustrate how the normal mode patterns shown in Fig. 11.4 are obtained. Note the numbers assigned to the oxygens in Fig. 11.4(b).

The search for the eigenvectors at the Γ point is similar to the procedure used for finding the normal modes of molecular vibration (see Sect. 8.3). Since $k = 0$, the phase factors for the translational symmetries are all $e^{i\boldsymbol{k}\cdot\boldsymbol{\tau}} = 1$. One just needs to consider the unit cell as the "molecule", find the normal

modes, and the eigenvectors will be a repetition of the normal modes in all the unit cells in the lattice.

From the character table for O_h we note that the characters for C_4^z are different for the Γ_{15} and Γ_{25} modes, and for this reason C_4^z is a useful symmetry operation for finding the normal mode displacements. First we consider the effect of C_4^z on each of the three inequivalent oxygen sites and on each of the three components of the vector; this consideration is independent of the symmetry of the vibrational mode:

$$C_4^z \begin{pmatrix} 1 \\ 2 \\ 3 \end{pmatrix} = \begin{pmatrix} 2 \\ 1 \\ 3 \end{pmatrix}, \quad C_4^z \begin{pmatrix} x \\ y \\ z \end{pmatrix} = \begin{pmatrix} y \\ -x \\ z \end{pmatrix}. \tag{11.10}$$

Finding the normal mode for the acoustic translational branch is trivial (see Fig. 11.4a). The operations of (11.10) are now applied to find the normal modes in Fig. 11.4b and e. For the Γ_{25} displacements, Fig. 11.4b shows the motions for the z component of the mode. The partners are found by cyclic operations on (x, y, z) and atom sites (1, 2, 3), as given in (11.11). Then operation by C_4^z yields

$$C_4^z \begin{pmatrix} -x_2 + x_3 \\ y_1 - y_3 \\ -z_1 + z_2 \end{pmatrix} = \begin{pmatrix} -y_1 + y_3 \\ -x_2 + x_3 \\ -z_2 + z_1 \end{pmatrix} = \begin{pmatrix} 0 & -1 & 0 \\ 1 & 0 & 0 \\ 0 & 0 & -1 \end{pmatrix} \begin{pmatrix} -x_2 + x_3 \\ y_1 - y_3 \\ -z_1 + z_2 \end{pmatrix} \tag{11.11}$$

giving a character of -1 for C_4^z in the Γ_{25} representation. Performing representative operations on this normal mode will show that it provides a proper basis function for the Γ_{25} irreducible representation in the point group O_h.

Now consider the Γ_{15} normal mode given in Fig. 11.4e. The displacements shown in the diagram are for the z component of the mode. To achieve no motion of the center of mass, the actual displacements must be $-z_1 - z_2 + 2z_3$ for the three oxygens at positions 1, 2 and 3. Using cyclic permutations we obtain the three components of the mode given in (11.12). Then action of C_4^z yields

$$\begin{aligned} C_4^z \begin{pmatrix} 2x_1 - x_2 - x_3 \\ -y_1 + 2y_2 - y_3 \\ -z_1 - z_2 + 2z_3 \end{pmatrix} &= \begin{pmatrix} 2y_2 - y_1 - y_3 \\ x_2 - 2x_1 + x_3 \\ -z_2 - z_1 + 2z_3 \end{pmatrix} \\ &= \begin{pmatrix} 0 & 1 & 0 \\ -1 & 0 & 0 \\ 0 & 0 & 1 \end{pmatrix} \begin{pmatrix} 2x_1 - x_2 - x_3 \\ -y_1 + 2y_2 - y_3 \\ -z_1 - z_2 + 2z_3 \end{pmatrix}, \end{aligned} \tag{11.12}$$

so that the character for this Γ_{15} mode is $+1$, in agreement with the character for the C_4^z operation in the $\Gamma_{15,z}$ irreducible representation (see the character table for O_h). Operation with typical elements in each class shows this mode provides a proper basis function for Γ_{15}.

Clearly all the modes shown in Fig. 11.4 have partners x,y and z, so that collectively they are all the normal modes for $BaTiO_3$. Since all modes for

$BaTiO_3$ at $\boldsymbol{k} = 0$ have odd parity, none are Raman-active, noting that for the O_h point group, Raman-active modes have A_g, E_g and T_{2g} (or Γ_1, Γ_{12} and $\Gamma_{25'}$) symmetries. However, the $3\Gamma_{15}$ or $3\Gamma_{15}^-$ modes are *infrared-active*, and can be excited when the $\boldsymbol{E}$ vector for the light is polarized in the direction of the oscillating dipole moment, as indicated in Fig. 11.4.

11.3.3 Phonons in the Nonsymmorphic Diamond Structure

We now illustrate the mode symmetries at the Γ point for a nonsymmorphic space group with 2 atoms/unit cell (specifically we illustrate the lattice modes of Ge or Si, which both crystallize in the diamond structure). Most of the symmetry properties, including the calculation of $\chi^{\text{equiv.}}$ and the decomposition of $\Gamma^{\text{equiv.}}$ into irreducible representations of O_h ($\Gamma^{\text{equiv.}} = \Gamma_1 + \Gamma_{2'}$), were discussed in Sect. 10.8. We now make use of this result for $\Gamma^{\text{equiv.}}$ in discussing the Γ point phonons.

To get the characters for the lattice vibrations, we then take $\Gamma_{\text{vec.}} = \Gamma_{15}$ which is odd under the inversion operation:

$$\Gamma_{\text{lat. mod.}} = \Gamma^{\text{equiv.}} \otimes \Gamma_{\text{vec.}} = (\Gamma_1 + \Gamma_{2'}) \otimes \Gamma_{15} = \Gamma_{15} + \Gamma_{25'} \,, \tag{11.13}$$

where $\Gamma_{25'}$ and $\Gamma_{2'}$ are respectively, even and odd under the inversion operation.

For each $\boldsymbol{k}$ value, there are six vibrational degrees of freedom with 2 atoms/unit cell. These break up into two triply degenerate modes at $\boldsymbol{k} = 0$, one of which is even, the other odd under inversion. The odd mode Γ_{15} is the acoustic mode, which at $\boldsymbol{k} = 0$ is the pure translational mode. The other mode is a $\Gamma_{25'}$ mode, which is symmetric under inversion and represents a breathing or optic mode. The optic mode is Raman-active but not infrared-active. Furthermore, the Raman-active mode is observed only with *off-diagonal polarization* $\boldsymbol{E}_{\text{i}} \perp \boldsymbol{E}_{\text{s}}$ for the incident and scattered light.

Let us now illustrate a screw axis operation in the diamond structure (see Fig. 9.6(g)) and see how this operation is used in finding the normal modes in a nonsymmorphic crystal. Denoting the dark atoms in Fig. 10.6 by 1 and the light atoms by 2, consider the effect of $\{C_4^z|\boldsymbol{\tau}\}$ on atom sites $\begin{pmatrix} 1 \\ 2 \end{pmatrix}$ and on the vector $\begin{pmatrix} x \\ y \\ z \end{pmatrix}$

$$\{C_4^z|\boldsymbol{\tau}\} \begin{pmatrix} 1 \\ 2 \end{pmatrix} = \begin{pmatrix} 2 \\ 1 \end{pmatrix} \,, \quad \{C_4^z|\boldsymbol{\tau}\} \begin{pmatrix} x \\ y \\ z \end{pmatrix} = \begin{pmatrix} y \\ -x \\ z \end{pmatrix} \,. \tag{11.14}$$

Using these results we can then obtain the characters for the displacements $(\boldsymbol{R}_1 + \boldsymbol{R}_2)$ which has Γ_{15} symmetry and is identified with the basic vibration of an FCC sublattice:

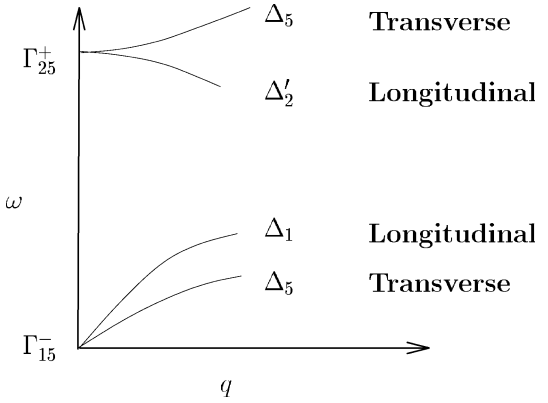

Fig. 11.5. Lattice modes along the Δ-axis for the diamond structure, showing the compatibility relations as we move away from the center of the cubic Brillouin zone

$$\{C_4^z|\boldsymbol{\tau}\}\begin{pmatrix} x_1+x_2 \\ y_1+y_2 \\ z_1+z_2 \end{pmatrix} = \begin{pmatrix} y_2+y_1 \\ -x_2-x_1 \\ z_2+z_1 \end{pmatrix} = \begin{pmatrix} 0\,1\,0 \\ -1\,0\,0 \\ 0\,0\,1 \end{pmatrix}\begin{pmatrix} x_1+x_2 \\ y_1+y_2 \\ z_1+z_2 \end{pmatrix} \tag{11.15}$$

yielding a character of $+1$ for $\{C_4^z|\boldsymbol{\tau}\}$, in agreement with the character for $\{C_4^z|\boldsymbol{\tau}\}$ in the Γ_{15} irreducible representation for the acoustic mode translational branches of point group O_h. If all the symmetry operations are then carried out, it is verified that $\boldsymbol{R}_1 + \boldsymbol{R}_2$ provides basis functions for the Γ_{15} irreducible representation of O_h.

When the two FCC sublattices vibrate out of phase, their parity is reversed and a mode with even parity (the $\Gamma_{25'}$ mode) is obtained

$$\{C_4^z|\boldsymbol{\tau}\}\begin{pmatrix} x_1-x_2 \\ y_1-y_2 \\ z_1-z_2 \end{pmatrix} = \begin{pmatrix} y_2-y_1 \\ -x_2+x_1 \\ z_2-z_1 \end{pmatrix} = \begin{pmatrix} 0 & -1 & 0 \\ 1 & 0 & 0 \\ 0 & 0 & -1 \end{pmatrix}\begin{pmatrix} x_1-x_2 \\ y_1-y_2 \\ z_1-z_2 \end{pmatrix} \tag{11.16}$$

yielding a character of -1. This checks with the character for $\{C_4^z|\boldsymbol{\tau}\}$ in the irreducible representation $\Gamma_{25'}$ for the point group O_h.

As we move away from $\boldsymbol{k} = 0$ along the Δ axis or the Λ axis, the triply degenerate modes break up into longitudinal and transverse branches. The symmetries for these branches can be found from the compatibility relations (see Sect. 10.7). For example, as we move away from $\boldsymbol{k} = 0$ along the Δ axis toward the X point (see Fig. 11.5), we have the compatibility relations

$$\begin{aligned} \Gamma_{15} &\rightarrow \Delta_1 + \Delta_5 \\ \Gamma_{25'} &\rightarrow \Delta_{2'} + \Delta_5\,. \end{aligned} \tag{11.17}$$

Group theory gives no information on the relative frequencies of the Γ_{15} and $\Gamma_{25'}$ modes.

We finally note that in general the Raman tensor has modes which transform as a second rank symmetric tensor (see Table 10.2). The Raman-active modes would include modes for the O_h group of the wave vector with symmetries $\Gamma_1 + \Gamma_{12} + \Gamma_{25'}$. Since the optic mode for the diamond structure at $k = 0$ has $\Gamma_{25'}$ symmetry, this mode is Raman-active. Table 10.2 also tells us that the $\Gamma_{25'}$ symmetry mode has basis functions of the form xy, yz, zx, indicating that the Raman tensor for the diamond structure is of the functional form $E_x^{\mathrm{i}} E_y^{\mathrm{s}}$; $\alpha_{xy}(\Gamma_{25'})$ plus cyclic permutations of x, y, z. Thus, observation of this Raman-active mode requires the use of cross-polarized light or $(\parallel, \perp)$ settings of the incident and scattered polarizations, respectively.

11.3.4 Phonons in the Zinc Blende Structure

Closely related to the diamond structure is the zinc blende structure (space group $F\overline{4}3m$ #216, T_d^3) where the two FCC sublattices in Fig. 10.6 are chemically distinct. This space group is symmorphic. This is the crystal structure for III–V semiconductor compounds, such as GaAs. For this case, the Ga atoms (ions) would be on one FCC sublattice and the As ions on the other FCC sublattice. If it happens that a Ga atom is on the wrong lattice, this is called an antisite location, and is considered a defect in the lattice.

Since the sublattices are chemically distinct, the group of the $\boldsymbol{k}$-vector at $\boldsymbol{k} = 0$ for the zinc blende structure has only the 24 operations of the point group T_d. It is a symmorphic structure and the factor group G_k/T_k is therefore isomorphic to its point group T_d (Sect. 9.1.4). In calculating $\Gamma_{\mathrm{lat.mod.}}$, we note that the vector in group T_d transforms as the irreducible representation Γ_{15}. Thus from the irreducible representations contained in $\Gamma^{\mathrm{equiv.}}$, we obtain

$$\Gamma^{\mathrm{equiv.}} = 2A_1 = 2\Gamma_1 \,,$$

so that when we take the direct product of $\Gamma^{\mathrm{equiv.}}$ with $\Gamma_{\mathrm{vec.}}$ we obtain

$$\Gamma_{\mathrm{lat.mod.}} = 2A_1 \otimes T_2 = 2T_2 = 2\Gamma_{15} \,. \tag{11.18}$$

For the zinc blende structure, the optic mode is both infrared-active and Raman-active since the irreducible representation Γ_{15} for point group T_d corresponds to both Γ_{15} and $\Gamma_{25'}$ of the point group O_h. This correspondence is apparent from comparing the character tables for T_d and O_h (see Table 10.2).

The well known LO–TO splitting of the optic phonon in ionic crystals is associated with an anticrossing of the optic phonon level and the photon propagation dispersion relation which occurs very close to the B.Z. center (see discussion in Sect. 10.7). Appropriate linear combinations of wave functions

will lead to two distinct levels that do not cross, each represented by the movement of one sublattice. Since GaAs is a polar crystal, in this case, the LO and TO modes will be split. The more polar the crystal, the larger the LO–TO splitting.

11.4 Lattice Modes Away from $\boldsymbol{k} = 0$

Modes at $\boldsymbol{k} \neq 0$ can be observed by optical spectroscopy when superlattice effects are present, giving rise to zone folding, or when defects are present, breaking down translational symmetry. Nonzone center modes can also be observed in second-order Raman spectra (comprising phonons with wave vectors $+\boldsymbol{k}$ and $-\boldsymbol{k}$). Lattice modes at $\boldsymbol{k} \neq 0$ are routinely observed by neutron, X-ray and electron inelastic scattering techniques.

To construct phonon branches for the entire range of $\boldsymbol{k}$ vectors within the first Brillouin zone, we must consider the general procedure for finding the lattice modes at other high symmetry points in the B.Z., and we make use of compatibility relations to relate these solutions to related solutions at neighboring $\boldsymbol{k}$-points.

The procedure for finding lattice modes at $\boldsymbol{k} \neq 0$ is outlined below:

(a) Find the appropriate group of the wave vector at point $\boldsymbol{k}$.
(b) Find $\Gamma^{\text{equiv.}}$ and $\Gamma_{\text{vec.}}$ for this group of the wave vector. When considering lattice modes away from the Γ point, care must be taken with special k points at the Brillouin zone boundary where $R_\alpha^{-1}\boldsymbol{k} = \boldsymbol{k} + \boldsymbol{K}_m$ ($\boldsymbol{K}_m$ is a reciprocal lattice vector). One should not simply use $\chi^{\text{equiv.}} = 1$ or 0, as for the case of molecules, because the lattice vector translation for $k \neq 0$ will add a phase factor (see Sect. 10.5). In this case we use for the characters for the equivalence transformation

$$\chi^{\text{equiv.}} = \sum_j \delta_{R_\alpha \boldsymbol{r}_j, \boldsymbol{r}_j} \mathrm{e}^{\mathrm{i}\boldsymbol{K}_m \cdot \boldsymbol{r}_j} \,, \tag{11.19}$$

where $\boldsymbol{r}_j$ is the position of the jth atom with respect to the origin of the point group, and $\delta_{R_\alpha \boldsymbol{r}_j, \boldsymbol{r}_j} = 1$ if $R_\alpha \boldsymbol{r}_j$ and $\boldsymbol{r}_j$ refer to equivalent atomic positions ($R_\alpha \boldsymbol{r}_j = \boldsymbol{r}_j + R_n$).
(c) Within a unit cell

$$\Gamma_{\text{lat.mod.}} = \Gamma^{\text{equiv.}} \otimes \Gamma_{\text{vec.}} \tag{11.20}$$

find the symmetry types and mode degeneracies of $\Gamma_{\text{lat.mod.}}$.
(d) Introduce a phase factor relating unit cells with translation by $\boldsymbol{\tau}$:

$$P_{\{\varepsilon|\tau\}} \Psi_k(\boldsymbol{r}) = \mathrm{e}^{\mathrm{i}\boldsymbol{k}\cdot\boldsymbol{\tau}} \Psi_k(\boldsymbol{r}) \quad \text{Bloch theorem} \,. \tag{11.21}$$

(e) Find lattice modes (including phase factor).

We illustrate these issues in terms of the NaCl structure which was previously considered with regard to its normal modes at $\boldsymbol{k} = 0$ (see Sect. 11.3.1).

11.4.1 Phonons in NaCl at the X Point $k = (\pi/a)(100)$

The group of the wave vector at the point X is given in the Table C.15 in Appendix C. We first identify the symmetry operations of point group D_{4h} and we then obtain $\Gamma^{\text{equiv.}}$ for these symmetry operations.

We first review the situation for the Γ point (O_h), see Table 11.2. Thus, we have $\Gamma^{\text{equiv.}}$ for the Na and Cl ions, and for $\Gamma_{\text{vec.}}$ at $k = 0$

$$\begin{aligned} \Gamma_{\text{Na}}^{\text{equiv.}} &= \Gamma_1 \\ \Gamma_{\text{Cl}}^{\text{equiv.}} &= \Gamma_1 \\ \Gamma_{\text{vec.}} &= \Gamma_{15}\,, \end{aligned}$$

so that for $k = 0$ we have

$$\Gamma_{\text{lat.mod.}} = 2\Gamma_1 \otimes \Gamma_{15} = 2\Gamma_{15}\,.$$

Similarly for the X point, we first find $\Gamma^{\text{equiv.}}$ for each type of atom (see Table 11.3). Thus, we obtain $\Gamma^{\text{equiv.}}$, $\Gamma_{\text{vec.}}$, and $\Gamma_{\text{lat.mod.}}$ at the X point:

$$\begin{aligned} \Gamma_{\text{Na}}^{\text{equiv.}} &= X_1 \\ \Gamma_{\text{Cl}}^{\text{equiv.}} &= X_1 \\ \Gamma_{\text{vec.}} &= X_4' + X_5'\,, \end{aligned}$$

where X_4' corresponds to x, and X_5' corresponds to (y, z). We thus obtain

$$\Gamma_{\text{lat.mod.}} = 2X_1 \otimes (X_4' + X_5') = 2X_4' + 2X_5'\,.$$

Compatibility relations give $\Gamma_{15} \to \Delta_1 + \Delta_5 \to X_4' + X_5'$ for the phonon branch connecting Γ to X.

The action of the translation operator on a basis function (normal mode) yields

$$\hat{P}_{\{\varepsilon|\tau\}} u(\boldsymbol{r}) = \mathrm{e}^{\mathrm{i}\boldsymbol{k}\cdot\boldsymbol{\tau}} u(\boldsymbol{r})\,, \tag{11.22}$$

Table 11.2. Characters for $\Gamma^{\text{equiv.}}$ for NaCl at the Γ point

Γ point	E	$8C_3$	$3C_4^2$	$6C_2'$	$6C_4$	i	$8iC_3$	$3iC_4^2$	$6iC_2'$	$6iC_4$
$\Gamma_{\text{Na}}^{\text{equiv.}}$	1	1	1	1	1	1	1	1	1	1
$\Gamma_{\text{Cl}}^{\text{equiv.}}$	1	1	1	1	1	1	1	1	1	1

Table 11.3. Characters for $\Gamma^{\text{equiv.}}$ for NaCl at the X point

X point	E	$2C_{4\perp}^2$	$C_{4\parallel}^2$	$2C_{4\parallel}$	$2C_2$	i	$2iC_{4\perp}^2$	$iC_{4\parallel}^2$	$2iC_{4\parallel}$	$2iC_2$
$\Gamma_{\text{Na}}^{\text{equiv.}}$	1	1	1	1	1	1	1	1	1	1
$\Gamma_{\text{Cl}}^{\text{equiv.}}$	1	1	1	1	1	1	1	1	1	1

where $\boldsymbol{k} = (\pi/a)\hat{x}$ at the X point under consideration. For $\boldsymbol{R}_n = a\hat{x}$ we obtain $\mathrm{e}^{i\boldsymbol{k}\cdot\boldsymbol{\tau}} = \mathrm{e}^{i\pi} = -1$ so that there is a π phase difference between unit cells along $\hat{x}$. However, for $\boldsymbol{R}_n = a\hat{y}$ or $a\hat{z}$, we have $\mathrm{e}^{i\boldsymbol{k}\cdot\boldsymbol{\tau}} = \mathrm{e}^{i(0)} = 1$, and there is effectively no phase factor along $\hat{y}$ and $\hat{z}$.

The phase factor of (11.22) refers to the relative phase in the vibration between atoms in adjacent unit cells. The relative motion between atoms within a unit cell was considered in Sect. 11.2. Thus the NaCl structure (space group #225) has a set of three acoustic branches and three optical branches each having X_4' and X_5' symmetries at the X point, where

$$X_4' \to x\,,$$
$$X_5' \to y, z\,.$$

The normal modes for the three acoustic branches are shown in Fig. 11.6 in terms of the symmetry classifications X_4' and X_5' (twofold) for the longitudinal and transverse branches, respectively. The corresponding normal modes for the three optical branches are shown in Fig. 11.7.

For rows of atoms in unit cells along the y and z directions, even considering that the crystal is strictly not infinite, there will be essentially *zero* phase difference ($\mathrm{e}^{i\delta a}$, with $\delta = \pi/N$, where $N \approx 10^7$) between molecules vibrating

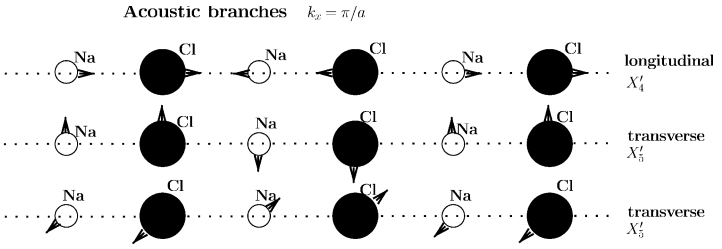

Fig. 11.6. Acoustic vibrational modes of NaCl showing longitudinal and transverse normal mode displacements at the X point ($k_x = \pi/a$) in the Brillouin zone for the X_4' and X_5' normal modes

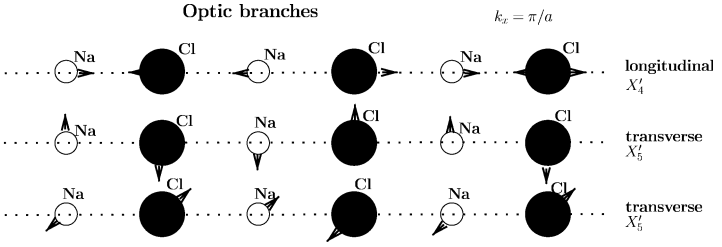

Fig. 11.7. Optic vibrational modes of NaCl showing longitudinal and transverse normal mode displacements at the X point ($k_x = \pi/a$) in the Brillouin zone for the X_4' and X_5' normal modes

in the acoustic mode as we move in the y and z directions. This is also true for the optical branches shown in Fig. 11.7.

11.4.2 Phonons in $BaTiO_3$ at the X Point

The modes in the case of $BaTiO_3$ (see Fig. 9.7(c)) involve more than one atom of the same species within the unit cell so that a few new aspects enter the lattice mode problem in this case. The character table for the group of the wave vector at the X point for $BaTiO_3$ is the same as for NaCl (Table C.15). At the X point, we compute $\Gamma^{\text{equiv.}}$ (see Table 11.4) using the symmetry operators for the group of the wave vector at the X point making use of the notation in Fig. 11.8.

$$\begin{aligned}
\Gamma^{\text{equiv.}}_{\text{Ba}} &= X_1 \\
\Gamma^{\text{equiv.}}_{\text{Ti}} &= X_1 \\
\Gamma^{\text{equiv.}}_{\text{O}_3} &= 2X_1 + X_2 \\
\Gamma_{\text{vec.}} &= X'_4 + X'_5 \,,
\end{aligned} \tag{11.23}$$

where X'_4 corresponds to x, and X'_5 to (y, z). The symmetries of the normal modes are found by taking the direct product of $\Gamma^{\text{equiv.}} \otimes \Gamma_{\text{vec.}}$

$$\begin{aligned}
\Gamma^{\text{Ba}}_{\text{lat.mod.}} &= X_1 \otimes (X'_4 + X'_5) = X'_4 + X'_5 \\
\Gamma^{\text{Ti}}_{\text{lat.mod.}} &= X_1 \otimes (X'_4 + X'_5) = X'_4 + X'_5 \,.
\end{aligned}$$

The Ba and Ti atoms form normal modes similar to NaCl with the Ba moving along x (X'_4 symmetry) or along y or z (X'_5 symmetry) with the Ti and O_3 at rest, and likewise for the Ti atoms moving along the x direction. The phase relations for atomic vibrations in adjacent unit cells in the x direction have a phase factor $e^{\pi i} = -1$, while rows of similar atoms in the y and z direction have no phase shift. For the oxygens,

$$\Gamma^{\text{O}_3}_{\text{lat.mod.}} = (2X_1 + X_2) \otimes (X'_4 + X'_5) = 2X'_4 + X'_3 + 3X'_5 \,. \tag{11.24}$$

The mode patterns and basis functions at the X point for $BaTiO_3$ are given in Fig. 11.8 and Table 11.5.

Table 11.4. Characters for the equivalence transformation for the Ba, Ti and three oxygen ions in $BaTiO_3$ with O_h symmetry

X point	E	$2C^2_{4\perp}$	$C^2_{4\parallel}$	$2C_{4\parallel}$	$2C_2$	i	$2iC^2_{4\perp}$	$iC^2_{4\parallel}$	$2iC_{4\parallel}$	$2iC_2$
$\Gamma^{\text{equiv.}}_{\text{Ba}}$	1	1	1	1	1	1	1	1	1	1
$\Gamma^{\text{equiv.}}_{\text{Ti}}$	1	1	1	1	1	1	1	1	1	1
$\Gamma^{\text{equiv.}}_{\text{O}_3}$	3	3	3	1	1	3	3	3	1	1

The mode symmetry and the normal mode displacements are verified by the following considerations. Perusal of the X-point character table shows that the symmetry types are uniquely specified by the operations $C_{4\|}, C_2$ and i. The effect of these operations on the coordinates (x, y, z) and on the site locations are

$$C_{4\|}\begin{pmatrix}1\\2\\3\end{pmatrix} = \begin{pmatrix}1\\3\\2\end{pmatrix}, \quad C_{4\|}\begin{pmatrix}x\\y\\z\end{pmatrix} = \begin{pmatrix}x\\-z\\y\end{pmatrix},$$

$$C_2\begin{pmatrix}1\\2\\3\end{pmatrix} = \begin{pmatrix}1\\3\\2\end{pmatrix}, \quad C_2\begin{pmatrix}x\\y\\z\end{pmatrix} = \begin{pmatrix}-x\\z\\y\end{pmatrix},$$

$$i\begin{pmatrix}1\\2\\3\end{pmatrix} = \begin{pmatrix}1\\2\\3\end{pmatrix}, \quad i\begin{pmatrix}x\\y\\z\end{pmatrix} = \begin{pmatrix}-x\\-y\\-z\end{pmatrix}.$$

By carrying out the symmetry operations on the basis functions, we verify that the matrix representations for each of the symmetry operations have the correct characters for the X_4' irreducible representation:

$$\begin{aligned} C_{4\|}(x_1 + x_2 + x_3) &= (x_1 + x_3 + x_2), \quad \text{so that} \quad \chi^{(C_{4\|})} = +1, \\ C_2(x_1 + x_2 + x_3) &= -(x_1 + x_3 + x_2), \quad \text{so that} \quad \chi^{(C_2)} = -1, \\ i(x_1 + x_2 + x_3) &= -(x_1 + x_2 + x_3), \quad \text{so that} \quad \chi^{(i)} = -1. \end{aligned}$$

Applying the same approach to the normal mode displacements with X_5' symmetry we have

$$C_{4\|}\begin{pmatrix}y_1+y_2+y_3\\z_1+z_2+z_3\end{pmatrix} = \begin{pmatrix}-z_1-z_3-z_2\\y_1+y_3+y_2\end{pmatrix} = \begin{pmatrix}0&-1\\1&0\end{pmatrix}\begin{pmatrix}y_1+y_2+y_3\\z_1+z_2+z_3\end{pmatrix}$$

$$i\begin{pmatrix}y_1+y_2+y_3\\z_1+z_2+z_3\end{pmatrix} = \begin{pmatrix}-1&0\\0&-1\end{pmatrix}\begin{pmatrix}y_1+y_2+y_3\\z_1+z_2+z_3\end{pmatrix},$$

so that $\chi(C_{4\|}) = 0$, and $\chi(i) = -2$, which are the correct characters for the X_5' irreducible representation. Finally for the X_3' modes

$$\begin{aligned} C_{4\|}(-x_2 + x_3) = (-x_3 + x_2) = -(-x_2 + x_3) &\rightarrow \chi(C_{4\|}) = -1 \\ C_2(-x_2 + x_3) = x_3 - x_2 = (-x_2 + x_3) &\rightarrow \chi(C_2) = +1 \\ i(-x_2 + x_3) = -(-x_2 + x_3) &\rightarrow \chi(i) = -1. \end{aligned}$$

These same calculations can be applied to the basis functions in Fig. 11.8 and their irreducible representations and the results are listed in Table 11.5.

The phase factors for oxygens separated by a lattice vector $a\hat{x}$ are $e^{\pi i} = -1$ while the oxygens separated by a lattice vector $a\hat{y}$ or $a\hat{z}$ have no phase difference (i.e., phase factor $\equiv 1$).

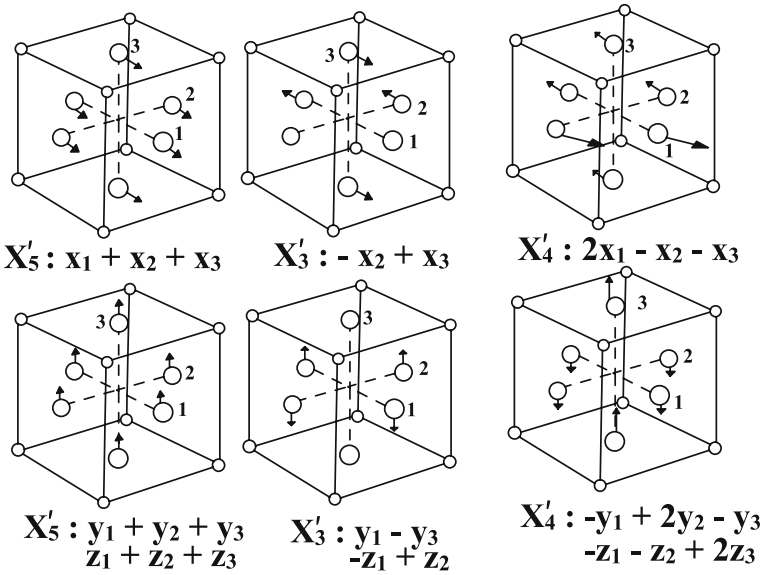

Fig. 11.8. Mode pattern models for the X point modes in $BaTiO_3$. The basis functions for each normal mode are indicated

Table 11.5. Basis functions for the various irreducible representations entering the lattice modes in $BaTiO_3$

basis functions	irreducible representation
$x_3 - x_2$	X_3'
$y_1 - y_3$ $-z_1 + z_2$	X_5'
$2x_1 - x_2 - x_3$	X_4'
$-y_1 + 2y_2 - y_3$ $-z_1 - z_2 + 2z_3$	X_5'
$x_1 + x_2 + x_3$	X_4'
$y_1 + y_2 + y_3$ $z_1 + z_2 + z_3$	X_5'

11.4.3 Phonons at the K Point in Two-Dimensional Graphite

Two-dimensional graphite, called a graphene sheet, belongs to the symmorphic hexagonal space group #191 of the International Tables of Crystallography [58] and has the symmetry designations D_{6h}^1 in accord with the Schoenflies notation, and $P6/mmm$ in the Hermann–Mauguin notation. Three-dimensional graphite is described by the nonsymmorphic space group #194

and symmetry designation D_{6h}^4 as is discussed further in Problem 11.1. Although a single graphene sheet is two-dimensional, we need to consider a three-dimensional space group to account for the out-of-plane phonons. The rotational aspects for real space and for the group of the wave vector at $k = 0$ in reciprocal space are described by the point group D_{6h} (see Fig. 11.9) and Table A.21. The direct lattice vectors are given by

$$\begin{aligned} \boldsymbol{a}_1 &= \frac{a}{2}\left(\sqrt{3}\hat{x} + \hat{y}\right) \\ \boldsymbol{a}_2 &= \frac{a}{2}\left(-\sqrt{3}\hat{x} + \hat{y}\right) , \end{aligned} \tag{11.25}$$

where $a = 2.456\,\text{Å}$ is the lattice parameter denoting the nearest neighbor distance between crystallographically equivalent atoms. The dotted line in Fig. 11.9a defines the rhombus for the real space unit cell containing two inequivalent carbon atoms, *labeled* 1 and 2. The associated Wyckoff positions for atoms 1 and 2 are

$$\begin{aligned} 1 &= (2/3, 1/3) \\ 2 &= (1/3, 2/3) . \end{aligned} \tag{11.26}$$

Figure 11.9b shows the hexagonal Brillouin zone of 2D graphite. The reciprocal lattice vectors are given by

$$\begin{aligned} \boldsymbol{b}_1 &= \frac{2\pi}{a}\left(\frac{\sqrt{3}}{3}\hat{k}_x + \hat{k}_y\right) \\ \boldsymbol{b}_2 &= \frac{2\pi}{a}\left(-\frac{\sqrt{3}}{3}\hat{k}_x + \hat{k}_y\right) . \end{aligned} \tag{11.27}$$

The letters Γ, $\boldsymbol{M}$ and $\boldsymbol{K}$ are the high symmetry points while Σ, T, and λ denote arbitrary points along high symmetry lines, and u represents a general point inside the two-dimensional Brillouin zone. The K point is a special symmetry point where the electronic valence and conduction bands cross in a single point through which the Fermi level passes. Before developing the group theory for the K point phonons, however, it is interesting to point out that, for the hexagonal Bravais lattice, the real and reciprocal lattice are rotated by 90° with respect to each other (see Fig. 11.9), and this is reflected in the definition of the symmetry axes (Fig. 11.10).

The appropriate group of the wave vector at the K point is the D_{3h} (see Table A.14). The $\Gamma_{\text{vec.}}$ transforms as $A_2^{''}$ for light polarized along the z-axis, and as E' for light polarized in the (x, y) plane. The $\chi^{\text{equiv.}}$ and $\Gamma^{\text{equiv.}}$ are given in Table 11.6. The characters for $\chi^{\text{equiv.}}$ in Table 11.6 are given by the number of atoms in the unit cell that remain unchanged under a symmetry operation for each class, except for $\chi^{\text{equiv.}}(C_3)$, since the C_3 operation takes the $\boldsymbol{k} = \boldsymbol{K}$ vector into an equivalent point, i.e., $C_3^{-1}\boldsymbol{K} = \boldsymbol{K} + \boldsymbol{K}_m$, where

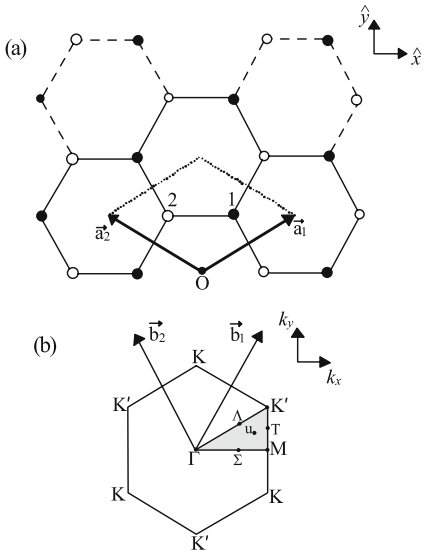

Fig. 11.9. Real (**a**) and reciprocal (**b**) lattices for a two-dimensional graphene sheet. The lattice vectors for real and reciprocal space are indicated and the two nonequivalent atoms with the real space unit cell are indicated in (**a**)

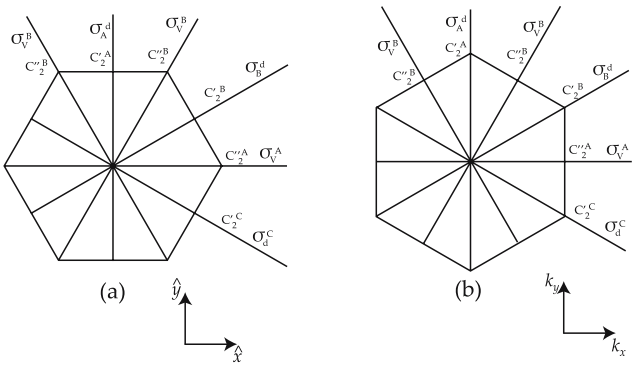

Fig. 11.10. (**a**) Directions of some symmetry operations of 2D graphite in the direct space. (**b**) Directions of some symmetry operations of 2D graphite in the reciprocal space

Table 11.6. $\Gamma^{\text{equiv.}}$ for the K point in graphite (D_{3h})

D_{3h}	E	$2C_3$	$3C_2$	σ_h	$2S_3$	$3\sigma_v$	
$\chi_K^{\text{equiv.}}$	2	−1	0	2	−1	0	$\Gamma_K^{\text{equiv.}} = E'$

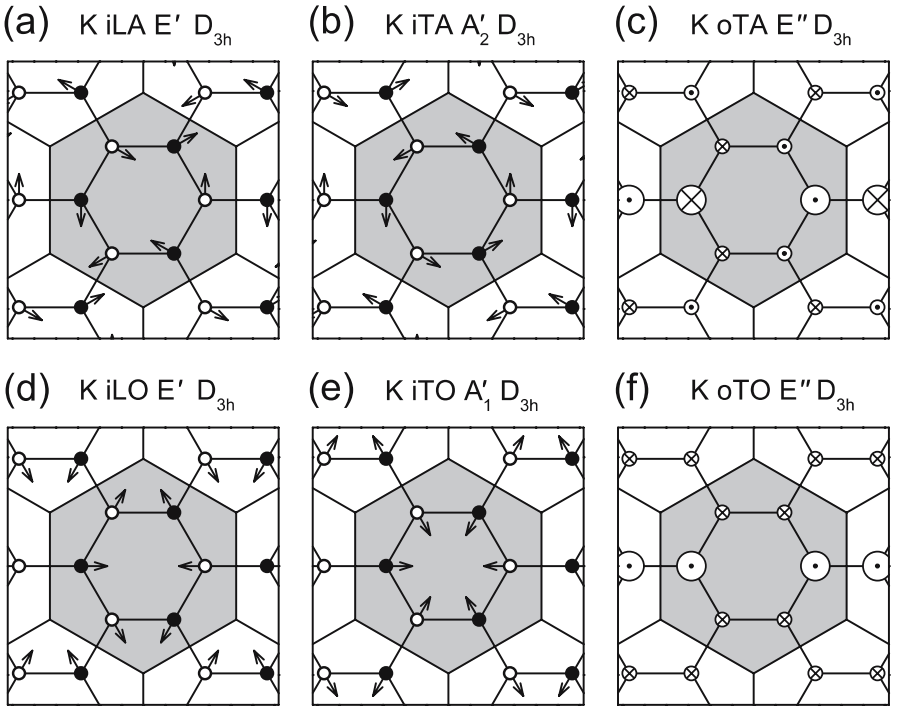

Fig. 11.11. A single graphene sheet. The solid and open dots indicate the A and B sublattices, respectively. The arrows show directions of the atomic displacements for the six stationary phonon modes of the graphene sheet at the K point. The labels of the phonon modes are identified in the text. The dotted and crossed points in (c) and (f) represent the vectors pointing in and out of the image plane. The large and small points indicate the magnitudes of the vectors equal to $\sqrt{2}$ and $1/\sqrt{2}$, respectively

$\boldsymbol{K}_m$ is a reciprocal lattice vector. The equivalence transformation is therefore given by (11.19), where $j = 1, 2$, and $\boldsymbol{r}_1 = (a/2)[(\sqrt{3}/3)\hat{x} + \hat{y}]$ and $\boldsymbol{r}_2 = (a/2)[(-\sqrt{3}/3)\hat{x} + \hat{y}]$. Considering the K point at $\boldsymbol{K} = (\boldsymbol{b}_1 + \boldsymbol{b}_2)/3)$, and considering $C_3^{-1}\boldsymbol{K} = \boldsymbol{K} - \boldsymbol{b}_1$ and from (11.19) we have for the equivalence representation (see Sect. 11.4)

$$\chi^{\text{equiv.}}(C_3) = \mathrm{e}^{i\boldsymbol{b}_1\cdot\boldsymbol{r}_1} + \mathrm{e}^{i\boldsymbol{b}_2\cdot\boldsymbol{r}_2} = \mathrm{e}^{-i4\pi/3} + \mathrm{e}^{-i2\pi/3} = 2\cos 2\pi/3 = -1\,, \quad (11.28)$$

as shown in Table 11.6 and a similar result follows for $S_3^{-1}K$. Finally,

$$\Gamma_{\text{lat.mod.}} = \Gamma^{\text{equiv.}} \otimes \Gamma_{\text{vec.}} = E' \otimes (A_2^{''} + E') = A_1^{'} + A_2^{'} + E' + E''\,. \quad (11.29)$$

There are four eigenvalues at the K point; two are nondegenerate and two are doubly degenerate.

The eigenvectors can be found from the projector algebra (see Sect. 4.3) by introducing a phase factor relating unit cells with translations by $\boldsymbol{R_n} = n_1\boldsymbol{a}_1 + n_2\boldsymbol{a}_2$, according to (11.21).

Figure 11.11 shows the normal mode displacements in the graphene sheet at the K point. When considering the D_{3h} symmetry and introducing the K point phase factor, the K point wavefunction periodicity is described by a supercell of six carbon atoms, as shown in gray in Fig. 11.11 (the lattice distortions caused by the K point phonon mode is incommensurate with the two-atom unit cell). The A_1' and A_2' phonon modes shown in Figs. 11.11 (b) and (e) obey C_6 symmetry, while the E' and E'' phonon modes in Figs. 11.11 (a), (d), and (f) have the C_2 rotation axes perpendicular to the hexagonal plane. In contrast, the point group D_{3h} contains the C_3 rotation axis, but neither the C_6 nor C_2 rotation axes. This contradiction is resolved by considering that the complex travelling phonon modes at the K (K′) point only have the C_3 rotation axes. Time-reversal symmetry mixes the complex travelling phonon modes at the K and K′ points into real stationary phonon modes that obey D_{6h} symmetry. The stationary phonon modes shown in Figs. 11.11 thus preserve the C_6 and C_2 rotation axes.

11.5 Phonons in Te and α-Quartz Nonsymmorphic Structures

In this section we discuss phonon modes for tellurium (with 3 atoms/unit cell). We then show how the lattice modes for this nonsymmorphic structure can be used to obtain the lattice modes for α-quartz (with 9 atoms/unit cell) which has the same space group as Te.

11.5.1 Phonons in Tellurium

The structure for Te (space groups $P3_121'$, #152; $P3_221'$, #154) is a spiral nonsymmorphic space group as shown in Fig. 11.12. There are three Te atoms/unit cell and these Te atoms are at levels 0, $c/3$ and $2c/3$. The structure for right-handed Te shows a right-handed screw when viewed along $+\hat{z}$. When the atoms are arranged with the opposite screw orientation, we have

Table 11.7. Character Table for the D_3 Point Group

D_3 (32)			E	$2C_3$	$3C_2'$
x^2+y^2, z^2		A_1	1	1	1
	R_z, z	A_2	1	1	−1
(xz, yz) (x^2-y^2, xy)	(x, y) (R_x, R_y)	E	2	−1	0

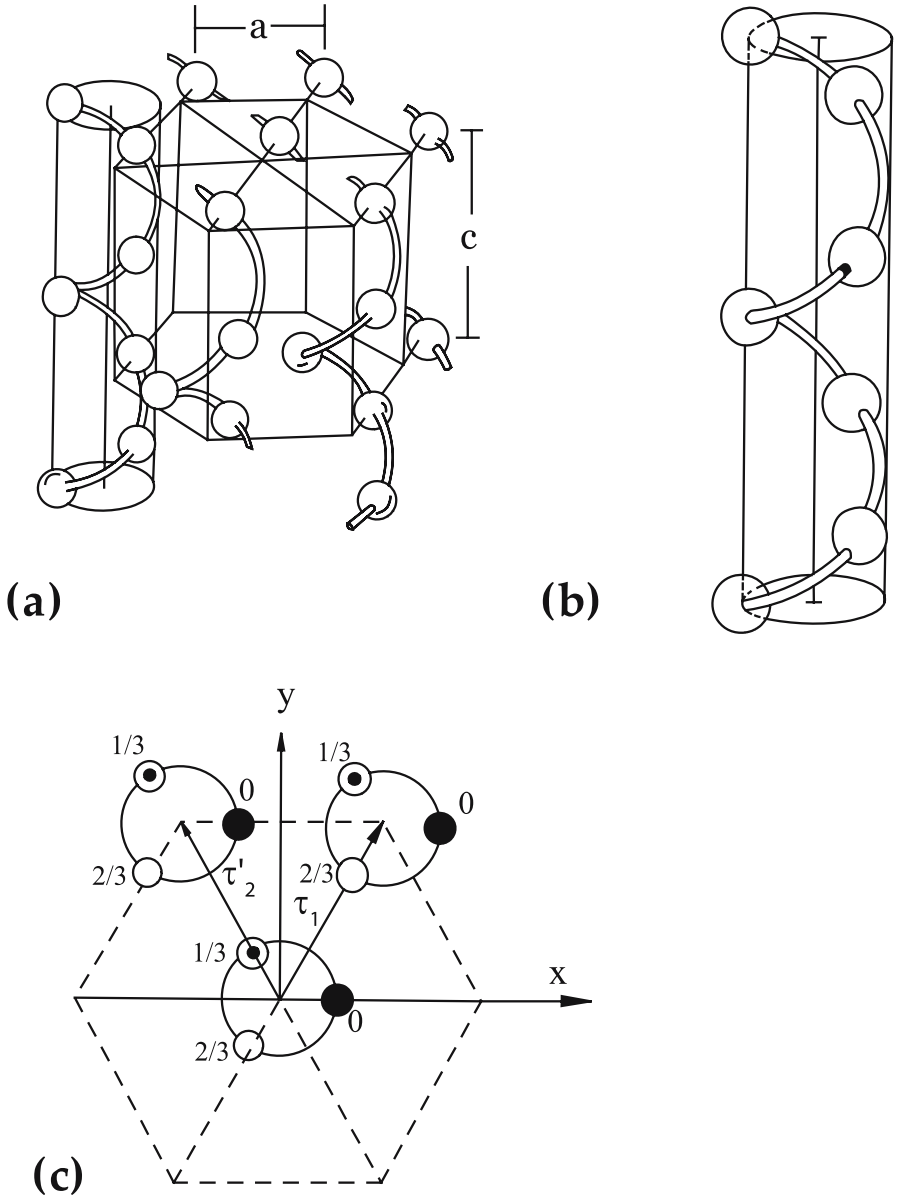

Fig. 11.12. (**a**) Model for the Te crystal structure showing the overall structure, (**b**) the structure of one chain from the side view, and (**c**) the top view of three adjacent chains Fix labels a, b, c on figure

Table 11.8. Characters for the Equivalence Transformation for the Group of the Wave Vector at $k = 0$ for Tellurium

	$\{E\|0\}$	$2\{C_3\|\boldsymbol{\tau}\}$	$3\{C_{2'}\|0\}$	
$\chi^{\text{equiv.}}$	3	0	1	$\Gamma^{\text{equiv.}} = A_1 + E$

left-handed Te. For this structure threefold rotations about the c axis must be combined with a translation $\boldsymbol{\tau} = (c/3)(001)$ to leave the crystal invariant. The three twofold symmetry axes normal to the threefold axis do not require translations. The appropriate point group at $\boldsymbol{k} = 0$ is D_3 and the character table is given in Table 11.7. Note that mirror planes are not symmetry operations.

Following the same procedure as was used for the nonsymmorphic diamond structure (see Sect. 11.3.3), we find $\Gamma^{\text{equiv.}}$ by considering the number of sites within the unit cell that remain invariant (or transform into the identical site in a neighboring unit cell, see Table 11.8). To find the lattice vibrations, we note that the vector transforms as $A_2 + E$. This allows us to separate out the lattice modes in the z-direction from those in the $x - y$ plane. For the *z-direction*

$$\Gamma^{\text{equiv.}} \otimes \Gamma_{\text{vec. z}} = (A_1 + E) \otimes A_2 = A_2 + E\,, \tag{11.30}$$

where the A_2 mode corresponds to pure translations in the z direction at $\boldsymbol{k} = 0$. The phonon dispersion curves for tellurium have been measured [61] by inelastic neutron scattering and the results along the high symmetry axes are shown in Fig. 11.13.

We show the normal modes with A_2 and E symmetry in Fig. 11.14. For the in-plane motion, the symmetries are obtained by computing:

$$\Gamma^{\text{equiv.}} \otimes \Gamma_{\text{vec. }(x,y)} = (A_1 + E) \otimes E = E + (A_1 + A_2 + E)\,. \tag{11.31}$$

The translational mode in the x, y directions transforms as E. The in-plane modes at $\boldsymbol{k} = 0$ are shown in Fig. 11.15. The A_2 and E modes are IR active, and the A_1 and E modes are Raman-active.

Since the Te structure has a screw axis, right and left circularly polarized light are of importance for optical experiments. For linear polarization, we consider the $\boldsymbol{E}$ vector for the light in terms of x, y, z components. For circular polarization we take the linear combinations $(x + iy)$ and $(x - iy)$. From the character table, we note that $(x + iy)(x - iy) = x^2 + y^2$ transforms as A_1 and the dipole moment $\boldsymbol{u}$ is related to the polarizability tensor $\overleftrightarrow{\alpha}$ by

$$\begin{pmatrix} (u_x + iu_y)/\sqrt{2} \\ (u_x - iu_y)/\sqrt{2} \\ u_z \end{pmatrix} = \begin{pmatrix} \alpha_{11}\ \alpha_{12}\ \alpha_{13} \\ \alpha_{21}\ \alpha_{22}\ \alpha_{23} \\ \alpha_{31}\ \alpha_{32}\ \alpha_{33} \end{pmatrix} \begin{pmatrix} (E_x + iE_y)/\sqrt{2} \\ (E_x - iE_y)/\sqrt{2} \\ E_z \end{pmatrix}, \tag{11.32}$$

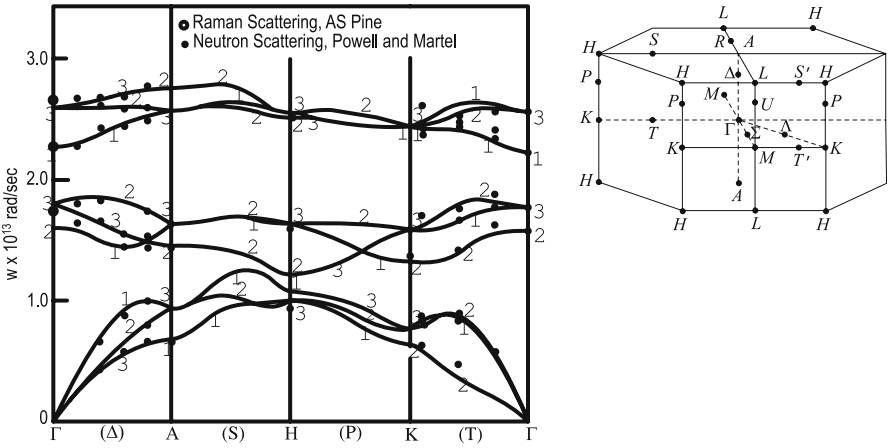

Fig. 11.13. Phonon modes for Te shown on the left along several high symmetry directions as indicated on the right (A.S. Pine and G. Dresselhaus, PRB Vol 4, p 356 (1971))

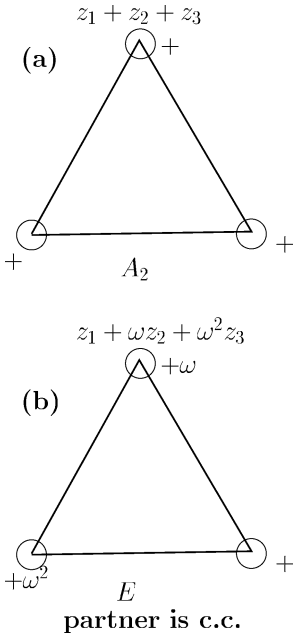

Fig. 11.14. Normal modes for Te for z-axis vibrations. The A_2 mode (**a**) is a pure translational mode along the z-axis. The E mode has displacements along z which have phase differences of $\omega = \exp(2\pi i/3)$ with respect to one another. One partner of the E mode is shown explicitly in (**b**). For the other partner, the displacements correspond to the interchange of $\omega \leftrightarrow \omega^2$, yielding the complex conjugate (c.c.) of the mode that is shown

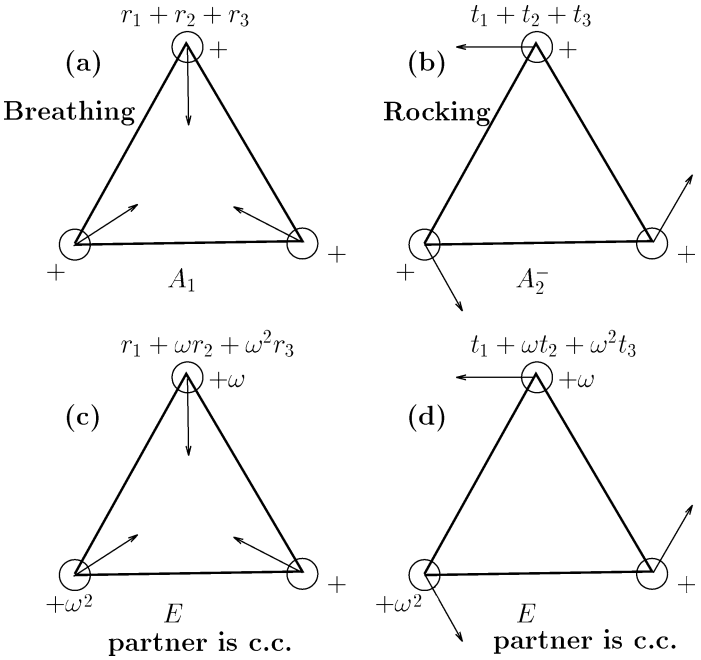

Fig. 11.15. In-plane normal modes for Te. The A_1 normal mode (**a**) is a breathing mode, while the A_2 mode (**b**) is a rocking mode corresponding to rotations of the three tellurium atoms for each half cycle of the vibration. The two E modes (**c**, **d**) can be described as a breathing and a rocking mode with phase relations $\omega = \exp(2\pi i/3)$ between each of the atoms as indicated (with the complex conjugate partner in each case obtained by the interchange of $\omega \leftrightarrow \omega^2$)

so that the polarizability tensor for A_1 modes will have the form

$$\overleftrightarrow{\alpha}_{A_1'} = \begin{pmatrix} a & 0 & 0 \\ 0 & a & 0 \\ 0 & 0 & 0 \end{pmatrix}$$

for in-plane motion with the Raman tensor having components $(E_+^{\mathrm{i}} E_-^{\mathrm{s}} + E_-^{\mathrm{i}} E_+^{\mathrm{s}})\alpha(A_1)$. The polarizability tensor for the z-axis motion is

$$\overleftrightarrow{\alpha}_{A_1''} = \begin{pmatrix} 0 & 0 & 0 \\ 0 & 0 & 0 \\ 0 & 0 & b \end{pmatrix}$$

and has A_1 symmetry with the Raman tensor having components $E_z^{\mathrm{i}} E_z^{\mathrm{s}} \alpha(A_1)$. Finally for general A_1 motion, the polarizability tensor is written as

$$\overleftrightarrow{\alpha}_{A_1} = \begin{pmatrix} a & 0 & 0 \\ 0 & a & 0 \\ 0 & 0 & b \end{pmatrix} . \tag{11.33}$$

To find the energy for aligning the dipole moment in an electric field, we need to take the dot product of the dipole moment with the electric field

$$\boldsymbol{E}^* \cdot \boldsymbol{u} = \left(\left[E_x - iE_y \right] / \sqrt{2}, \left(E_x + iE_y \right) / \sqrt{2}, E_z \right) \cdot \begin{pmatrix} (u_x + iu_y)/\sqrt{2} \\ (u_x - iu_y)/\sqrt{2} \\ u_z \end{pmatrix} ,$$

so that

$$\begin{aligned} \boldsymbol{E}^* \cdot \boldsymbol{u} &= (E_-, E_+, E_z) \cdot \begin{pmatrix} u_+ \\ u_- \\ u_z \end{pmatrix} \\ &= E_- u_+ + E_+ u_- + E_z u_z = E_x u_x + E_y u_y + E_z u_z = \text{real quantity} . \end{aligned}$$

For the electromagnetic (infrared) interaction, the pertinent symmetries are $E_+ u_-(E) + E_- u_+(E)$ for in-plane motion and $E_z u_z(A_2)$ for z-axis motion.

In considering the Raman effect, we find the energy of the Raman interaction in terms of $\boldsymbol{E}^* \cdot \overleftrightarrow{\alpha} \cdot \boldsymbol{E}$ which, when properly symmetrized becomes $1/2 \left[\boldsymbol{E}^* \cdot \overleftrightarrow{\alpha} \cdot \boldsymbol{E} + \boldsymbol{E} \cdot \overleftrightarrow{\alpha}^* \cdot \boldsymbol{E}^* \right]$. Thus for the Raman mode with A_1 symmetry, the induced dipole u_+ has the same sense of polarization as the incident electric field. However, the energy involves $\boldsymbol{E}_{\mathrm{i}}^*$ and $\boldsymbol{E}_{\mathrm{s}}$ or alternatively $\boldsymbol{E}_{\mathrm{s}}^*$ and $\boldsymbol{E}_{\mathrm{i}}$ to yield the combination $(1/2)(E_+^{\mathrm{i}} E_-^{\mathrm{s}} + E_-^{\mathrm{i}} E_+^{\mathrm{s}})$ which transforms as $(x + iy)(x - iy) = x^2 + y^2$, as desired for a basis function with A_1 symmetry.

For Raman modes with E symmetry we can have a dipole moment u_z induced by E_+, leading to the combination of electric fields $E_z^* E_+$. To have a symmetric polarizability tensor, we must also include the term $(E_z^* E_+)^* = E_- E_z$ since the energy must be unchanged upon interchange of electric fields $\boldsymbol{E} \leftrightarrow \boldsymbol{E}^*$. Thus the polarizability and Raman tensors must be of the form

$$\overleftrightarrow{\alpha}_{E,1} = \begin{pmatrix} 0 & 0 & 0 \\ 0 & 0 & r^* \\ r & 0 & 0 \end{pmatrix} , \quad \text{and} \quad \begin{cases} E_+^{\mathrm{i}} E_z^{\mathrm{s}} \alpha_-(E) + E_-^{\mathrm{i}} E_z^{\mathrm{s}} \alpha_+(E) \\ \text{or } E_z^{\mathrm{i}} E_+^{\mathrm{s}} \alpha_-(E) + E_z^{\mathrm{i}} E_-^{\mathrm{s}} \alpha_+(E) . \end{cases} \tag{11.34}$$

The partner of this polarizability tensor with E symmetry will produce the displacement u_z from an electric field displacement E_- yielding

$$\overleftrightarrow{\alpha}_{E,2} = \begin{pmatrix} 0 & 0 & r \\ 0 & 0 & 0 \\ 0 & r^* & 0 \end{pmatrix} . \tag{11.35}$$

The other lattice mode for Te with E symmetry (denoted here by E') produces a dipole moment u_+ from an electric field E_-. This however involves $E_-(E_+)^* = E_-^2$ for the incident and scattered electric fields so that the polarizability tensor in this case is

$$\overleftrightarrow{\alpha}_{E',1} = \begin{pmatrix} 0 & s & 0 \\ 0 & 0 & 0 \\ 0 & 0 & 0 \end{pmatrix} ; \quad \text{basis function} \quad x_-^2 \tag{11.36}$$

and the corresponding partner is

$$\overleftrightarrow{\alpha}_{E',2} = \begin{pmatrix} 0 & 0 & 0 \\ s^* & 0 & 0 \\ 0 & 0 & 0 \end{pmatrix} ; \quad \text{basis function} \quad x_+^2 \,. \tag{11.37}$$

The Raman tensor for the E' mode has the form $E_+^{\rm i} E_+^{\rm s} \alpha_+(E) + E_-^{\rm i} E_-^{\rm s} \alpha_-(E)$. We can relate these partners of the E' modes to the basis functions of the character table for D_3 by considering the basis functions for the partners

$$\begin{aligned} &\text{Partner \#1:} \quad \frac{1}{2}(x - iy)^2 = x_-^2 \\ &\text{Partner \#2:} \quad \frac{1}{2}(x + iy)^2 = x_+^2 \,. \end{aligned} \tag{11.38}$$

By taking the sums and differences of these partners we obtain

$$\begin{aligned} x_+^2 + x_-^2 &= \frac{1}{2}(x + iy)^2 + \frac{1}{2}(x - iy)^2 = (x^2 - y^2) \\ x_+^2 - x_-^2 &= \frac{1}{2}(x + iy)^2 - \frac{1}{2}(x - iy)^2 = 2xy \,, \end{aligned} \tag{11.39}$$

which form a set of partners listed in the character table for D_3.

11.5.2 Phonons in the α-Quartz Structure

We will now examine the lattice modes of α-quartz (space group D_3^4, #152, $P3_121$ for the right-hand crystal or D_3^5, #153, $P3_212$ for the left-hand crystal). We will use this example as a means for showing how lattice modes for crystals with several atoms per unit cell (such as α-quartz) can be built up from simpler units, in this case the tellurium structure discussed in Sect. 11.5.1. In Sect. 11.6 we discuss the effect of an applied axial compressive force upon lattice vibrations in α-quartz.

The spiral structure of α-quartz about the z-axis is shown in Fig. 11.16(a) where each solid ball represents a SiO_2 unit, and the diagram on the left is identical to that for tellurium (see Fig. 11.12(a)). The projection of the nine atoms in SiO_2 onto the basal plane is shown in Fig. 11.16(b). The Si

atoms (1, 4 and 7) occupy positions at levels 0, $c/3$, $2c/3$, respectively (as for tellurium). The oxygen atoms (9, 5, 3, 8, 6 and 2) occupy positions at levels $c/9$, $2c/9$, $4c/9$, $5c/9$, $7c/9$ and $8c/9$, respectively (these sites are of course not occupied in tellurium). Thus both Te and α-quartz are described by the same space group, but have different site symmetries. Figure 11.16 shows the right-handed tellurium structure.

There are three molecular SiO_2 units per unit cell giving rise to nine atoms per unit cell or *27 lattice branches* of which 24 are optic modes. By examining the atom locations in Fig. 11.16(b), we can determine the point group symmetry of α-quartz. The z-axis is a threefold axis of rotation when combined with the translation $\boldsymbol{\tau} = (c/3)(001)$. In addition there is a twofold axis from the center to each of the silicon atoms. The symmetry elements are the same as for tellurium discussed in Sect. 11.5.1. In order to determine the normal modes of vibration, we first find the characters for the transformation of the atomic sites. It is convenient to make use of the results for tellurium, noting that the silicon atoms in quartz occupy the same sites as in tellurium. In Table 11.9 we obtain the lattice modes in α-quartz at $\boldsymbol{k} = 0$.

The lattice modes for the silicon are identical with those found previously for Te, so that part of the problem is already finished. For the six oxygens we have

$$\Gamma_{\text{lat.mod.},\,z} = (A_1 + A_2 + 2E) \otimes A_2\,; \quad \text{for } z \text{ motion}$$

$$\Gamma_{\text{lat.mod.},\,x,y} = (A_1 + A_2 + 2E) \otimes E\,; \quad \text{for } x, y \text{ motion}\,.$$

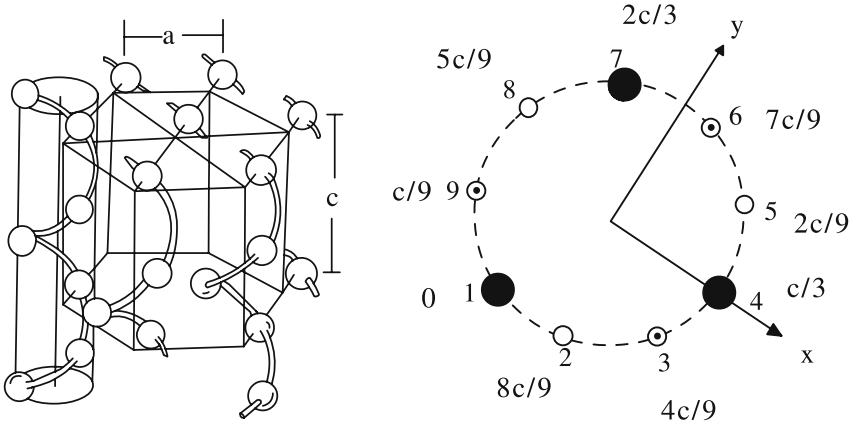

(a) (b)

Fig. 11.16. Structure of (**a**) right-handed α-quartz and (**b**) the projection of the atoms on the basal plane of α-quartz. Atoms #1, 4, 7 denote Si and the other numbers denote oxygen atoms

Table 11.9. Characters for the Equivalence Transformation for α-quartz

	$\{E\|0\}$	$2\{C_3\|\boldsymbol{\tau}\}$	$3\{C_2'\|0\}$	
$\Gamma_{\text{Si}}^{\text{equiv.}}$	3	0	1	$= A_1 + E$
$\Gamma_{\text{oxygen}}^{\text{equiv.}}$	6	0	0	$= A_1 + A_2 + 2E$

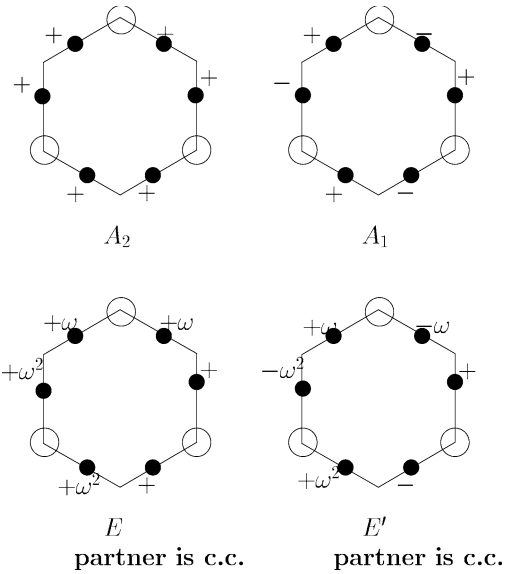

Fig. 11.17. Normal modes along the z-direction for the six oxygens in the α-quartz crystal. The A_2 mode is a uniform translation while the A_1 mode is a rocking of the oxygens around the Si. The E modes are related to the A_2 and A_1 modes by combining the $1, \omega, \omega^2$ phases with the translational and rocking motions

Carrying out the direct products we obtain

$$\begin{aligned} \Gamma_{\text{lat.mod.},\,z} &= A_2 + A_1 + 2E\,; \quad \text{for } z \text{ motion} \\ \Gamma_{\text{lat.mod.},\,x,y} &= 2A_1 + 2A_2 + 4E\,; \quad \text{for } x, y \text{ motion}\,, \end{aligned} \tag{11.40}$$

where we note that for the D_3 point group $E \otimes E = A_1 + A_2 + E$.

The corresponding z-axis normal modes A_2, A_1, E and E' for the six oxygens are shown in Fig. 11.17. The normal mode A_2 is clearly a uniform translation of the six oxygens, while the A_1 mode is a rocking of the two oxygens on either side of a silicon atom (one going up, while the other goes down). The twofold E mode is derived from A_2 by introducing phases $1, \omega, \omega^2$ for each of the pairs of oxygens around a silicon atom; the complex conjugate E mode is obtained from the one that is illustrated by the substitution $\omega \leftrightarrow \omega^2$. Finally the E' mode is obtained from the A_1 mode in a similar way as the

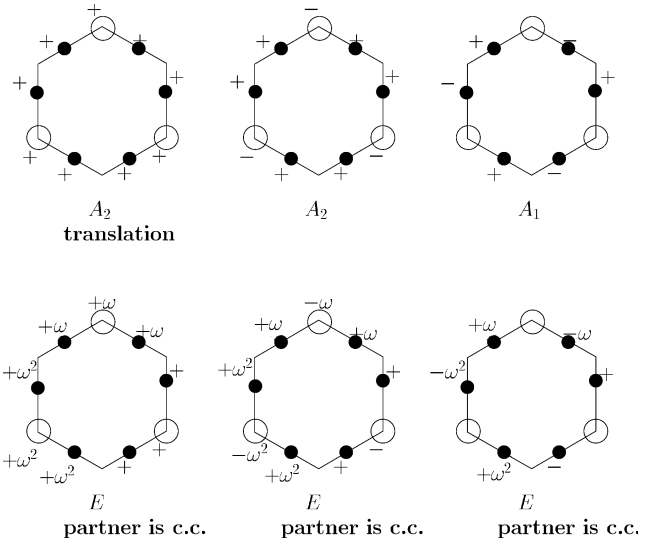

Fig. 11.18. Normal modes along the z-direction for the three SiO_2 groups in α-quartz. Here the motions of the Si atoms are combined with those of the oxygens

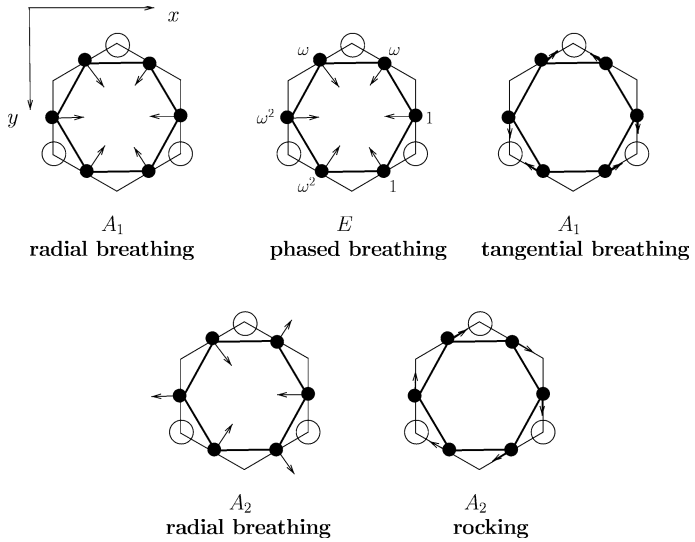

Fig. 11.19. Normal modes in the x–y plane for the six oxygens in the α quartz crystal. In addition, the A_1 tangential breathing mode, the A_2 radial breathing breathing mode, and the A_2 rocking mode have corresponding E modes, with phases $1, \omega, \omega^2$ for the three SiO_2 units, each having two partners related by $\omega \leftrightarrow \omega^2$. In the crystal, all modes with the same symmetry are coupled, so that the actual normal mode is an admixture of the modes pictured here

E mode is obtained from the A_2 mode. In identifying the symmetry type for these normal modes, we note the effect of symmetry operation C_2'.

We now combine the z motion for the silicons (symmetries A_2+E) with the z motion for the oxygens (symmetries A_1+A_2+2E) to obtain A_1+2A_2+3E for SiO_2. The resulting normal mode patterns are shown in Fig. 11.18. The z-axis translational mode for the six oxygens combine either in-phase or out of phase to form the two normal modes with A_2 symmetry. For the mode with A_1 symmetry, the silicon atoms remain stationary. Introducing the phases 1, ω, ω^2 for each SiO_2 group gives the three E normal modes along the z-direction in α-quartz.

For the xy motion, the six oxygens form lattice modes with symmetries $2A_1+2A_2+4E$ and the normal mode patterns are shown in Fig. 11.19.

The next step is to combine the motion of the silicon (A_1+A_2+2E) with that of the two oxygens ($2A_1+2A_2+4E$) for the in-plane modes, and this step is the focus of Problem 11.2.

11.6 Effect of Axial Stress on Phonons

In general, an external perturbation, when applied to a crystal, reduces the symmetry of the crystal. The fundamental principle used to deduce this lower symmetry is called the Curie principle which states that only those symmetry operations are allowed which are common to both the unperturbed system and to the perturbation itself. This condition restricts the new symmetry group to a subgroup common to the original group.

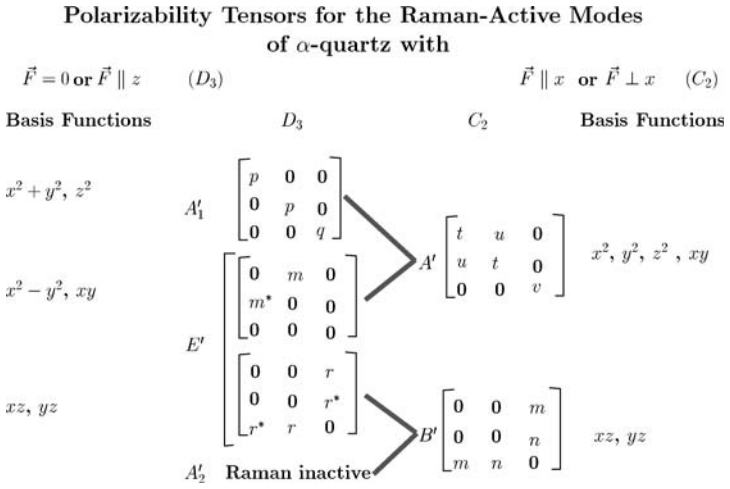

Fig. 11.20. The symmetry of the Polarizability Tensors for Raman Active Modes of α-quartz, for stress applied along the threefold axis, and along a twofold axis perpendicular to the threefold axis

When a homogeneous axial compression is applied to a crystal, the resulting strain is described by a symmetric tensor of the second rank. The strain tensor can be represented by an ellipsoid which has at least D_{2h} point group symmetry; if two of its major axes are equal, the ellipsoid acquires rotational symmetry about the third axis, and the point group symmetry is $D_{\infty h}$, whereas, if all three axes are equal it becomes a sphere with three-dimensional continuous rotation and reflection symmetry. In order to determine the symmetry operations of the strained crystal it is necessary to know the orientation of the strain ellipsoid relative to the crystallographic axes. An alternative procedure is to treat the stress itself as the imposed condition and to find the symmetry elements common to the unstrained crystal and to the symmetry of the stress tensor.

Using the symmetry properties of the stress tensor is particularly simple when the external perturbation is an axial compression. In this case the stress ellipsoid has $D_{\infty h}$ point group symmetry and can be conveniently represented by a right circular cylinder with its center coinciding with the center of the crystal and its axis of revolution along the direction of the force. The symmetry operations common to the unstrained crystal and to the cylinder representing the stress can then be easily determined by inspection.

As an illustrative case, consider the point group D_3, the point group of α-quartz (Sect. 11.5.2). The symmetry operations of D_3 are a threefold axis of rotation along the z-axis and three twofold axes perpendicular to the z-axis, one of which is taken to be the x-axis. If the force, $\boldsymbol{F}$, is applied along the z-direction, all of the operations of the group are common to the symmetry of the stress and hence the symmetry remains D_3. If, however, the force is applied along the x direction, the only remaining symmetry operation is C_2. Similarly, if the force is applied along the y-axis, the only remaining symmetry operation is again the twofold axis of rotation along the x-axis and the symmetry is reduced to the point group C_2. If the force is in a direction other than along z or parallel or perpendicular to a two-fold axis, the crystal symmetry is reduced to C_1.

Table 11.10. Character table for group C_2 pertinent to uniaxial deformation applied to D_3 symmetry group. The compatibility relations among their irreducible representations are also given

C_2 (2)			E	C_2	
x^2, y^2, z^2, xy	R_z, z	A	1	1	
xz, yz	x, y R_x, R_y	B	1	-1	
representations of D_3		A_1	1	1	A
		A_2	1	-1	B
		E	2	0	$A + B$

Once the reduced symmetry of the crystal in the presence of the external perturbation is determined, the correlation between the irreducible representations of the two groups can be obtained. From such a correlation, the removal of the degeneracy of a particular energy level can be immediately deduced as illustrated below for the force applied along the twofold axis.

This group theoretical analysis thus predicts that the Raman lines of E symmetry should split and the Raman inactive A_2 mode in D_3 symmetry should become Raman-active in C_2 symmetry. We note that the basis functions that are used for C_2 are x, y, z while for D_3, the combinations $(x + iy, x - iy, z)$ are used. The form of the polarizability tensors for the Raman-active modes in D_3 and C_2 point group symmetries are given in Fig. 11.20, and are further considered in Problem 11.2.

Selected Problems

11.1. This problem involves the lattice modes of a three-dimensional graphite crystal (see Fig. C.1).

(a) What are the symmetry operations for 3D crystalline graphite, and how do they differ from those for 2D graphite (see Sect. 11.4.3)?
(b) Why is the space group #194 appropriate for 3D hexagonal graphite, rather than #191, or #192, or #193?
(c) Find the number of lattice modes for 3D graphite at $k = 0$. What are their symmetries and what are their mode degeneracies?
(d) What are the normal mode displacements for each of these lattice modes at $k = 0$?
(e) Find the mode symmetries and compatibility relations for the modes in the $\Gamma - T - K$ direction (see Fig. 11.13). Be aware that the K point is a special point where the relation $R_\alpha k = k + K_m$ occurs (see Table C.27).
(f) Which modes in (e) are IR active, Raman active? What are the polarizations of the Raman active modes?
(g) Find the eigenvectors at the K point for 3D graphite.
(h) Compare the results for two-dimensional and three-dimensional graphite and discuss the difference in behavior in terms of the connection between symmorphic and nonsymmorphic groups.

11.2. Use the results given in Sect. 11.5.2 for the lattice modes of crystalline SiO_2 to do this problem.

(a) Find the normal modes for the in-plane vibrations of crystalline SiO_2 obtained by combining the lattice modes for the three Si atoms and for the six oxygen atoms given in Sect. 11.5.2. How many have A_1, A_2 and E symmetry? On the basis of your results explain the normal mode patterns given in Fig. 11.21 for the modes with A_1 and A_2 symmetry, and discuss the normal mode patterns for the E symmetry modes.

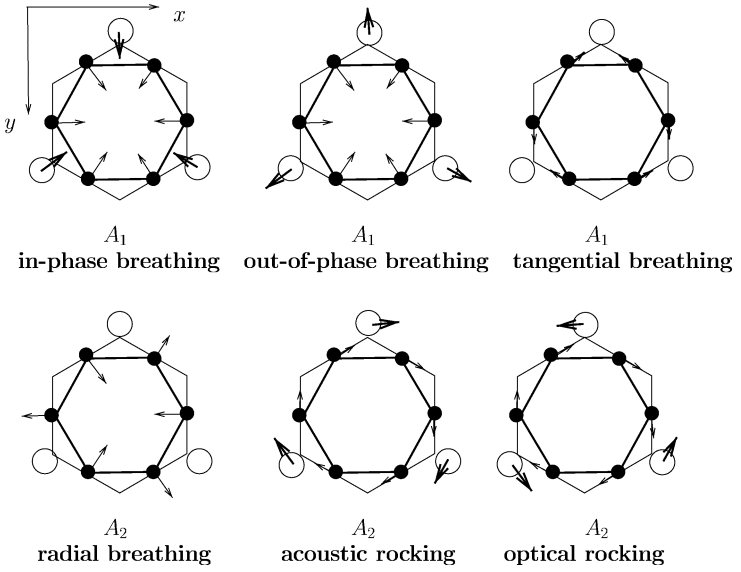

Fig. 11.21. The in-plane normal modes for α-quartz obtained by superposition of the normal modes for the oxygens and the silicons. Corresponding to each of the one-dimensional modes shown here are two-dimensional E modes with phases $1, \omega, \omega^2$ for the three SiO_2 units, with the two partners related by $\omega \leftrightarrow \omega^2$

(b) Suppose that a stress is applied along the c-axis, what is the effect on the normal mode patterns? Now suppose that a stress is applied along a twofold axis going through a Si atom, what is the effect on the normal mode patterns?

11.3. Consider the crystal structure in the diagram for Nb_3Sn, a prototype superconductor with the A–15 (or β–W) structure used for high field superconducting magnet applications [54, 76].

(a) How many lattice modes are there at $k = 0$, what are their symmetries and what are their degeneracies?
(b) What are the normal mode displacements for each of these lattice modes?
(c) Which modes are IR active, Raman active? What are the polarizations of the Raman-active modes?

11.4. Tin oxide (SnO_2 with space group #136) is an important electronic material [54, 76].

(a) Find the Wyckoff positions from the site positions of the Sn and O atoms in the unit cell. Find $\Gamma^{\text{equiv.}}$ for the SnO_2 structure.
(b) Find the lattice modes at $k = 0$, their symmetries, degeneracies and the normal mode patterns.
(c) Indicate the IR-activity and Raman activity of these modes.

11.5. Bromine forms a molecular crystal [54, 76].

(a) What is the appropriate space group? What are the Wyckoff positions for each of the distinct bromine atoms within the unit cell.
(b) Find the lattice modes at $k = 0$, their symmetries, degeneracies and the normal mode patterns.
(c) Indicate the IR-activity and Raman activity of these modes.

11.6. Carbon nanotubes are an interesting system where first-order Raman activity can be based on selection rules for the *electron–phonon* interaction [8]. The electronic states usually belong to two-dimensional irreducible representations (E_μ) and five types of allowed first-order resonance Raman scattering processes between $E_\mu^{(v)}$ and $E_{\mu'}^{(c)}$ can be obtained

$$
\begin{aligned}
&\text{(I)}\ E_\mu^{(v)} \xrightarrow{\mathrm{Z}} E_\mu^{(c)} \xrightarrow{\mathrm{A}} E_\mu^{(c)} \xrightarrow{\mathrm{Z}} E_\mu^{(v)}\,,\\
&\text{(II)}\ E_\mu^{(v)} \xrightarrow{\mathrm{X}} E_{\mu\pm1}^{(c)} \xrightarrow{\mathrm{A}} E_{\mu\pm1}^{(c)} \xrightarrow{\mathrm{X}} E_\mu^{(v)}\,,\\
&\text{(III)}\ E_\mu^{(v)} \xrightarrow{\mathrm{Z}} E_\mu^{(c)} \xrightarrow{\mathrm{E_1}} E_{\mu\pm1}^{(c)} \xrightarrow{\mathrm{X}} E_\mu^{(v)}\,,\\
&\text{(IV)}\ E_\mu^{(v)} \xrightarrow{\mathrm{X}} E_{\mu\pm1}^{(c)} \xrightarrow{\mathrm{E_1}} E_\mu^{(c)} \xrightarrow{\mathrm{Z}} E_\mu^{(v)}\,,\\
&\text{(V)}\ E_\mu^{(v)} \xrightarrow{\mathrm{X}} E_{\mu\pm1}^{(c)} \xrightarrow{\mathrm{E_2}} E_{\mu\mp1}^{(c)} \xrightarrow{\mathrm{X}} E_\mu^{(v)}\,,
\end{aligned}
\tag{11.41}
$$

where A, E_1, and E_2 denote phonon modes of different Γ-point symmetries of $\mu = 0$, $\mu = \pm1$, and $\mu = \pm2$, respectively. The XZ plane is parallel to the substrate on which the nanotubes lie, the Z axis is directed along the nanotube axis, and the Y-axis is directed along the light propagation direction, so that the Z and X in (11.41) stand for the light polarized parallel and perpendicular to the nanotube axis, respectively. The five processes of (11.41) result in different polarization configurations for different phonon modes: ZZ and XX for A, ZX and XZ for E_1, and XX for E_2.

(a) Derive the selection rules in (11.41) explicitly.
(b) The Raman active modes are those transforming like quadratic functions (XX, YY, ZZ, XY, YZ, ZX). The selection rules associated with the first and third arrows in (11.41) come basically from selection rules for the electron–photon interaction. Show that the selection rules for different polarizations obtained in (11.41) are in perfect agreement with the basis functions analysis.

11.7. Show that the Raman and infrared active modes in chiral and achiral carbon nanotubes are given by the following symmetries [8]:

$$
\begin{aligned}
\Gamma^{\text{Raman}}_{\text{zigzag}} &= 2A_{1g} + 3E_{1g} + 3E_{2g} \rightarrow 8\,\text{modes}\,,\\
\Gamma^{\text{infrared}}_{\text{zigzag}} &= A_{2u} + 2E_{1u} \rightarrow 3\,\text{modes}\,,\\
\Gamma^{\text{Raman}}_{\text{armchair}} &= 2A_{1g} + 2E_{1g} + 4E_{2g} \rightarrow 8\,\text{modes}\,,\\
\Gamma^{\text{infrared}}_{\text{armchair}} &= 3E_{1u} \rightarrow 3\,\text{modes}\,,\\
\Gamma^{\text{Raman}}_{\text{chiral}} &= 3A_1 + 5E_1 + 6E_2 \rightarrow 14\,\text{modes}\,,\\
\Gamma^{\text{infrared}}_{\text{chiral}} &= A_2 + 5E_1 \rightarrow 6\,\text{modes}\,.
\end{aligned}
\tag{11.42}
$$